



Kaunas University of Technology
Faculty of Mechanical Engineering and Design

UAV Signal Propagation Simulation in Normal and Hazardous Weather Conditions

Master's Final Degree Project

Agnė Simonavičiūtė

Project author

Assoc. Prof. dr. Saulius Japertas

Supervisor

Kaunas, 2020



Kaunas University of Technology

Faculty of Mechanical Engineering and Design

UAV Signal Propagation Simulation in Normal and Hazardous Weather Conditions

Master's Final Degree Project

Aeronautical Engineering (6211EX024)

Agnė Simonavičiūtė

Project author

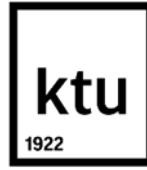
Assoc. Prof. dr. Saulius Japertas

Supervisor

Assoc. Prof. dr. Vitas Grimaila

Reviewer

Kaunas, 2020



Kaunas University of Technology

Faculty of Mechanical Engineering and Design

Agnė Simonavičiūtė

UAV Signal Propagation Simulation in Normal and Hazardous Weather Conditions

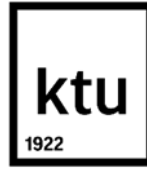
Declaration of Academic Integrity

I confirm that the final project of mine, Agnė Simonavičiūtė, on the topic „UAV signal propagation simulation in normal and hazardous weather conditions“ is written completely by myself; all the provided data and research results are correct and have been obtained honestly. None of the parts of this thesis have been plagiarized from any printed, Internet-based or otherwise recorded sources. All direct and indirect quotations from external resources are indicated in the list of references. No monetary funds (unless required by Law) have been paid to anyone for any contribution to this project.

I fully and completely understand that any discovery of any manifestations/case/facts of dishonesty inevitably results in me incurring a penalty according to the procedure(s) effective at Kaunas University of Technology.

(name and surname filled in by hand)

(signature)



Kaunas University of Technology
Faculty of Mechanical Engineering and Design
Study programme: Aeronautical Engineering (6211EX024)

Task of the Master's Final Degree Project

Given to the student: Agnė Simonavičiūtė

1. Title of the Project:

UAV Signal Propagation Simulation in normal and hazardous weather conditions

Bepiločio skraidymo aparato signalo sklidimo modeliavimas normaliomis ir pavojingomis oro sąlygomis.

2. Aim of the Project:

The aim of this project is to suggest the stochastic model predicting the losses of signal propagation in real-time using air-deployed UAV in atmospheric boundary layer.

3. Tasks of the Project:

1. to compare the air-deployed UAV system with the other weather data gathering systems;
2. to investigate the influence of shape of the air-deployed UAV system for the accuracy of gathered data;
3. to analyse the impact of weather phenomena to signal propagation;
4. to develop the body of air-deployed UAV system using simulation software;
5. to suggest the signal propagation model in normal and hazardous weather conditions.

4. Approbation:

Part of Final degree project results were presented during the 23rd International Scientific Conference Transport Means 2019, printed ISSN 1822-296 X.

4. Structure of the Text Part:

- Air-deployed UAV and alternative observation systems comparison.
- Effect of the shape investigation on the falling object.
- The impact analysis of weather phenomena to the UAV signal propagation.
- Air-Deployed UAV body evaluation.

- UAV signal propagation simulation.

Author of the Final Degree Project

Agnė Simonavičiūtė

(abbreviation of the position, name, surname, signature, date)

Supervisor of the Final Degree Project

Assoc. Prof. dr. Saulius Japertas

(abbreviation of the position, name, surname, signature, date)

Head of Study Programmes

prof. Artūras Keršys

(abbreviation of the position, name, surname, signature, date)

Agnė Simonavičiūtė. UAV Signal Propagation Simulation in Normal and Hazardous Weather Conditions. Master's Final Degree Project / supervisor Assoc. Prof. dr. Saulius Japertas; Faculty of Mechanical Engineering and Design, Kaunas University of Technology.

Study field and area (study field group): Aeronautical Engineering (E14), Engineering Science.

Keywords: Air-deployed UAV, Path losses, signal propagation.

Kaunas, 2020. 46 p.

Summary

The use of Unmanned Aerial Vehicles (UAV) areas is highly increasing. One of the newest use of the areas of the UAV is the research of meteorological characteristics. The research is very important and necessary in the presence of hazardous meteorological conditions. Currently such systems as radiosondes, dropsondes, weather radars, satellite systems, or human-piloted aircrafts are used, they have many advantages, and however, there are disadvantages as well.

The use of air-deployed UAV could expand the range of the research, but also the disadvantages of other previously mentioned systems could be avoided. Dropsonde is the most suitable system to gather data in low layers of the atmosphere, especially in storm clouds. Such a system could use the body of octahedron in a combination with a streamer tail.

The most common problem is the transmission of the gathered information to the ground station in real-time. It is related to radio waves, which transmit the information, sensitivity to various external factors such as humidity, temperature, noises, fading, etc. That is why it is necessary to anticipate the propagation of radio waves at the design stage of the air-deployed UAV which gathers and transmits the information in real-time.

In this research, based on the electromagnetic wave statistical characteristics, the losses of signal propagation are predicted, evaluating the influence of rain, clouds, and path losses. The proposed model is based on a normal distribution stochastic differential equation. This model can accurately describe the loss of the propagation path by selecting a free member ε , nevertheless, the predicted propagation losses are very sensitive to the change of the free member ε .

The created model is compared with the experimental results and with other authors' research. In this work, the measurement was made with the drone in normal weather conditions and in low altitudes. The results obtained demonstrate great compliance with the model.

Further analysis can concentrate on the full measurement of the low layer of the atmosphere achieving 2-3 km in both normal and hazardous weather conditions. These measurements are essential in creating ε alteration model.

The accomplished model was suggested during the 23rd International Scientific Conference Transport Means 2019.

Agnė Simonavičiūtė. Bepiločio skraidymo aparato signalo sklidimo modeliavimas normaliomis ir pavojingomis oro sąlygomis. Magistro baigiamasis projektas / vadovas doc. dr. Saulius Japertas; Kauno technologijos universitetas, Mechanikos inžinerijos ir dizaino fakultetas.

Studijų kryptis ir sritis (studijų krypčių grupė): Aeronautikos inžinerija (E14), Inžinerijos mokslai.

Reikšminiai žodžiai: Bepilotis skraidymo aparatas, kelio nuostoliai, signalo sklidimas.

Kaunas, 2020. 46 p.

Santrauka

Bepiločių skraidymo aparato panaudojimo sritys vis labiau ir labiau plečiasi. Viena iš naujesnių UAV panaudojimo sričių yra meteorologinių charakteristikų tyrimas. Tokie tyrimai ypač naudingi ir reikalingi esant sudėtingoms meteorologinėms sąlygoms. Šiuo metu naudojamos tokios priemonės, kaip aerozondai, oro radarai, palydovinės sistemos ar žmonių pilotuojami orlaiviai turi privalumų, bet ir nemažai trūkumų. UAV panaudojimas leistų ne tik praplėsti tokių tyrimų spektrą, bet ir išvengti daugelio trūkumų, kuriuos turi aukščiau minėtos sistemos.

Atlikus palyginimą, buvo nustatyta, kad iš oro paleisti bepiločiai skraidymo aparatai, yra tinkamiausi tyrinėti žemesnius atmosferos sluoksnius, ypač pavojinguose audros debesys. Šiai sistemai siūloma naudoti oktaedro korpusą, su integruota uodega, kad sulėtinti kritimą.

Didžiausia problema išlieka ne informacijos surinkimas iš sudėtingų meteorologinių sistemų, bet tos informacijos perdavimas realiame laike į antžeminę stotį. Tai susiję su radijo bangų, kuriomis perduodama informacija, jautrumo įvairiems išoriniams faktoriams: drėgnumui, temperatūrai, triukšmams, slopinimui ir t.t. Todėl tokių UAV, skirtų informacijos surinkimui ir perdavimui realiame laike, projektavimo stadijoje būtina numatyti radijo bangų sklidimą.

Šiame darbe, remiantis elektromagnetinių bangų statistiniu charakteriu, yra prognozuojami signalo sklidimo kelio nuostoliai, o gauti rezultatai palyginami su kitų autorių darbų eksperimentiniais rezultatais. Siūlomas modelis sukurtas remiantis normaliojo skirstinio stochastine diferencialine lygtimi.

Sukurtas modelis buvo palygintas su eksperimentiniais rezultatais ir su kitų autorių tyrimais. Šiame darbe matavimas buvo atliekamas su Bepiločiu orlaiviu normaliomis oro sąlygomis pasiekiant nedidelį aukštį. Gauti rezultatai rodo puikų modelio atitikimą su eksperimento duomenimis.

Tolimesnis tyrimas gali būti koncentruotas į pilną žemo atmosferos sluoksnio matavimą, pasiekiantį 2–3 km atstumą tiek normaliomis, tiek pavojingomis oro sąlygomis. Šie matavimai yra būtini kuriant ϵ pokyčio modelį.

Table of contents

Table of contents	8
List of figures	9
List of tables	10
List of abbreviations and terms	11
Introduction	12
1. Air-deployed UAV and alternative observation systems	14
1.1. Weather observation systems	14
1.1.1. Radiosonde	14
1.1.2. Meteorological radar systems.....	16
1.1.3. Weather Satellite systems.....	16
1.1.4. Aircraft-based observations.....	17
1.1.5. Unmanned Aerial Vehicles.....	18
1.1.6. Air-deployed UAV	19
1.2. Analysis of meteorological systems	19
2. The effect of the shape on the falling object	21
2.1. The motion of free-falling objects	21
2.2. Forces acting on a falling object.....	21
2.3. The effect of the drag on the shape	22
3. The impact of weather phenomena to the UAV signal propagation	24
3.1. Path losses	24
3.2. Rain impact.....	25
3.3. The influence of clouds	26
4. Air-Deployed UAV body analysis	28
4.1. Shape of the dropsonde evaluation.....	28
4.2. Drag coefficient analysis	28
4.3. Additional elements for slower descent	30
5. UAV signal propagation simulation	34
5.1. Stochastic equations	34
5.2. Path losses	35
5.3. Evaluation of the Wiener process.....	37
5.4. The influence of the Rain	37
5.5. The influence of clouds	38
5.6. Signal propagation PL predicting model.....	38
5.7. The measurement of the path losses.....	39
5.8. Analysis of the signal propagation model	39
Conclusions	42
Discussion	43
List of references	44
Appendices	47
Appendix 1. Coefficients of drag of the shapes.....	47

List of figures

Fig. 1. Global weather observation system (GOS) [4]	14
Fig. 2. Radiosonde system [8]	15
Fig. 3. The radar beam path with respect to height [13]	16
Fig. 4. Space-based observation system [4]	17
Fig. 5. Aircraft-based observations [18].....	18
Fig. 6. NCAR/Vaisala dropsonde [22]	19
Fig. 7. Air-deployed UAV system [24].....	20
Fig. 8. Drag coefficient according to the shape of the body [29].....	23
Fig. 9. Geometric shapes for analysis	28
Fig. 10. Velocity profiles of octahedron	31
Fig. 11. From left to right parachute, streamer, turbine wings. One directional steady flow.	32
Fig. 12. From left to right parachute, streamer, turbine wings. Side flow of the stream.	32
Fig. 13. From left to right parachute, streamer, turbine wings. Side-stream Vorticity.	33
Fig. 14. <i>PL</i> extrapolation to height (<i>h</i>), according to works [2], [3], [30] and [33].....	36
Fig. 15. Variation of the path losses in hazardous weather conditions	36
Fig. 16. Standard deviations for white noises model	37
Fig. 17. Noise in terms of path losses.....	37
Fig. 18. Experiment data compared with the model.....	39
Fig. 19. ε relation to path losses, when $\sigma = 2$ dB.....	40
Fig. 20. ε relation to path losses, when $\sigma = 6.2$ dB.....	40
Fig. 21. Cumulative distribution function	41
Fig. 22. Probability density function	41

List of tables

Table 1. Comparison of weather system.....	20
Table 2. Coefficient of Drag of the shapes	29
Table 3. Model parameters	38

List of abbreviations

Abbreviations:

ABL – atmospheric boundary layer.

AI – artificial intelligence.

CDF – cumulative distribution function.

CFD – Computational Fluid Dynamics.

GOS – global observation system.

PDF – probability density function.

PL – path losses.

UAV – unmanned aerial vehicle.

Introduction

The development of unmanned aircraft vehicles is highly increasing. It has led to expanded areas of system application. One of these areas is a meteorological research. The weather UAV that can gather weather data and information is being developed by the scientists. This system is especially required in the areas where the frequent storm occurs. It will help to provide real-time data of the state of the atmosphere to make weather forecasts more accurate. The controllable storm UAV will fly to desired locations of the atmosphere to deploy sensors to gather weather data, this will enable meteorologists to predict weather situations for a longer period of time.

Most of weather-related applications for UAV are only image related. It is important to develop small sensor carrying systems that can be deployed directly to the storm cloud, to expand these researches. It will help to detect even the smallest changes in the atmosphere. It is expected that these sensors will become part of the Global observation system and weather predictions will be more accurate. In this research the body of presumable Air-deployed UAV will be investigated.

The transmission of the signal to the ground station is the other issue when considering hazardous weather environment. There are only a few this kind of research analysing signal propagation in real-time. These studies are essential for the development of Air-deployed UAV because the signal suffers many obstacles while propagating through the atmosphere, especially in hazardous weather conditions including clouds and rain. The impact of the path losses will be evaluated during this research.

Novelty of the project

Although Air-deployed UAVs have been in use for a long time, some moments of their application in practice still require additional attention. This also applies to meteorological research using UAV [1-3]. The propagation of the radio signal under difficult meteorological conditions in real-time has not yet been fully investigated, this is evidenced by various works in this field.

Relevance of the topic

The meteorological data collected by meteorological Air-deployed UAV will help meteorologists to provide better weather forecasts. It is expected that the radiosondes will be included in World's Meteorological Organisations (WMO) Global Observation System (GOS). The accuracy of gathered data in real-time strongly depends on signal propagation, which is not yet fully investigated.

The aim of the project is:

to suggest the stochastic model predicting the losses of signal propagation in real-time using air-deployed UAV in the atmospheric boundary layer.

Approbation:

Part of Final degree project results, suggesting stochastic path losses predicting model, was presented during the 23rd International Scientific Conference Transport Means 2019, authors: Japertas S., Simonavičiūtė, A., Vencloviėnė, A., topic: UAV signal propagation simulation in hazardous weather conditions, printed: ISSN 1822-296 X.

The tasks are:

1. to compare the air-deployed UAV system with the other weather data gathering systems;
2. to investigate the influence of the shape of the air-deployed UAV system for the accuracy of gathered data;
3. to analyse the impact of weather phenomena to signal propagation;
4. to develop the body of air-deployed UAV system using simulation software's;
5. to suggest the signal propagation model in normal and hazardous weather conditions.

1. Air-deployed UAV and alternative observation systems

This project will investigate the atmospheric boundary layer (from 100 m to 3 km), where most of the weather phenomena, especially hazardous, occurs. Critical properties for this investigation are operating altitude, stability, and controllability of the system. To investigate the weather impact on signal propagation the vertical analysis of the atmosphere must be performed.

1.1. Weather observation systems

The World Meteorological Organization (WMO) international organization uniting meteorologists around the world, established the World Weather Watch programme, one of its core components is the Global Observing System (GOS), which purpose is to make meteorological observations. These observations gather meteorological data from different layers of the atmosphere, according to this, there are two main categories [4, 5]: Surface-based Observations and Space-based Observations. Each category uses different types of Observation systems.

GOS consists of multi-component observing systems [6]: satellite imagery and sensor data, combined with readings from ground-based observations and radars, manned flights and weather balloons, are gathered into complex weather data bases, then statistical models are created and processed by high-level performance computers (Fig. 1) are used for meteorological forecasting. Currently dropsondes are not involved in GOS.

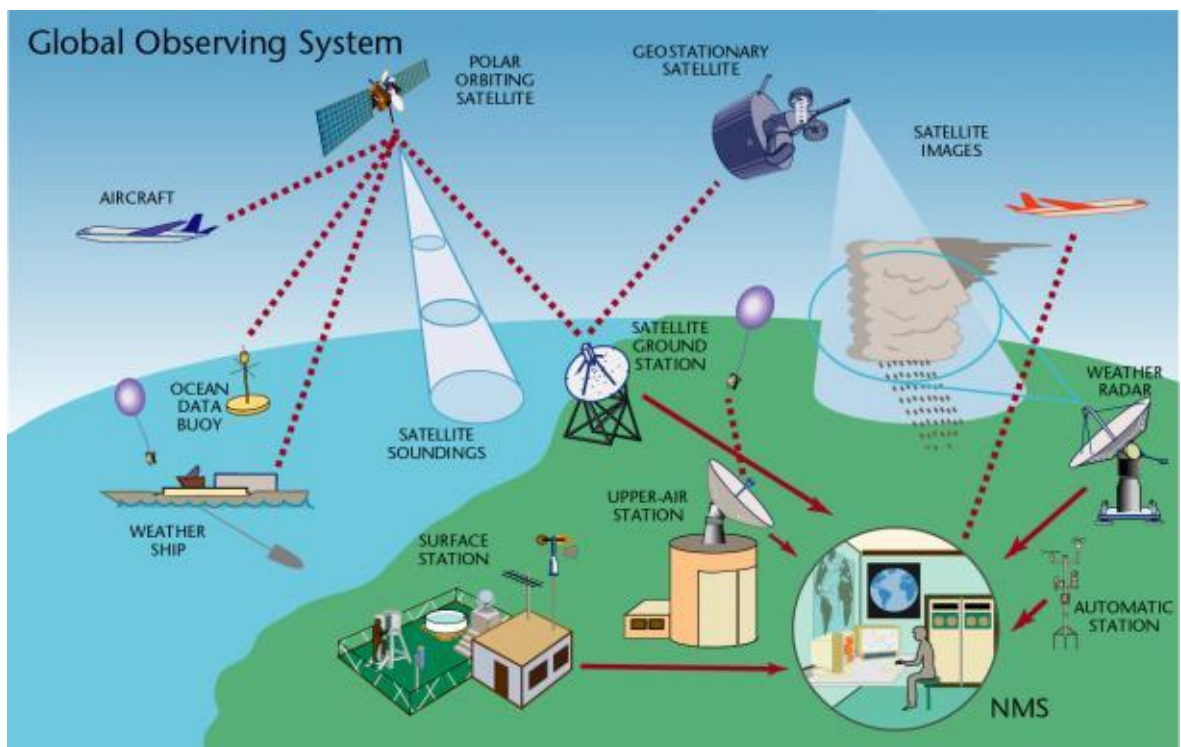


Fig. 1. Global weather observation system (GOS) [4]

1.1.1. Radiosonde

Radiosondes are UAV deployed from the surface (Fig. 2) carried by balloon filled with light-weighted gasses. It makes long-distance measurements collecting data in high altitudes of atmosphere, while drifted with the flow of the wind. The system provided quality and the precision of gathered data is hardly achieved by any other observation systems. Radiosondes are unique instruments as they

provide continuous, detailed profiles from the ground to altitudes of 10 km and above [7]. The reliability and accuracy of the measurements are very important. The smallest imprecision in the collected data can lead the forecaster to perceiving critical details and making correct conclusions.

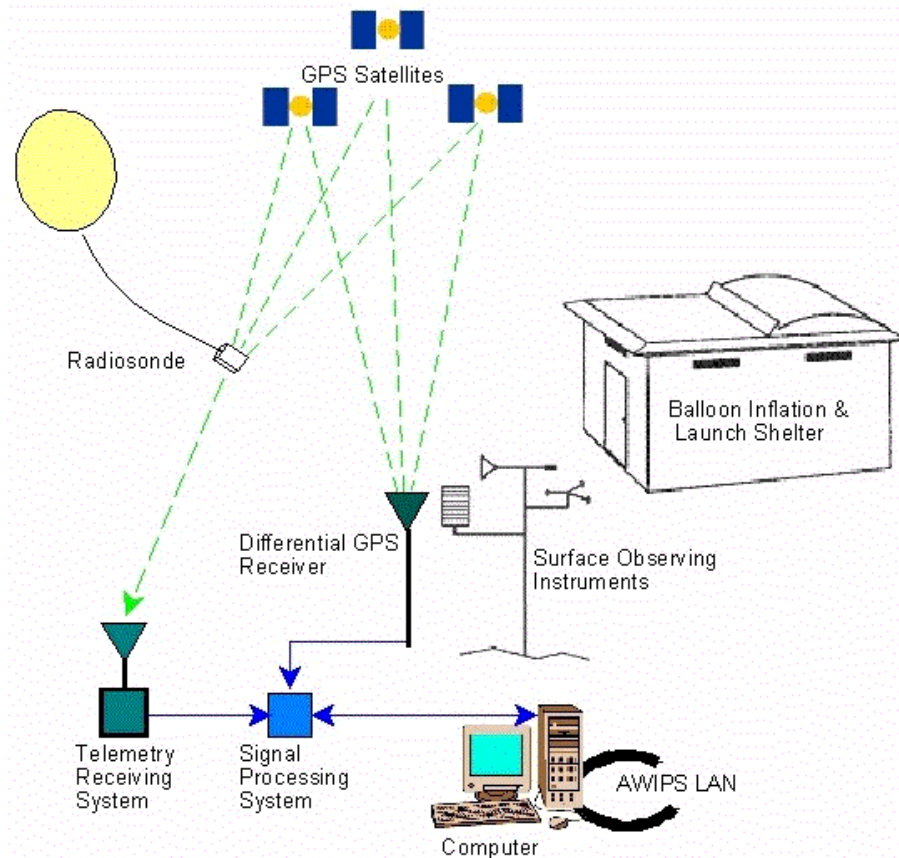


Fig. 2. Radiosonde system [8]

Traditional weather observation systems are becoming outdated [9, 10], especially when considering of tracking and forecasting the presence of storm clouds. When the radiosonde is released from the ground, the system travels together with the stream of the wind, passing the lower layers of the atmosphere quickly. As a result, it is difficult for the meteorologists to record important meteorological data vertically. Also, the weather balloon lacks the ability of controllability, it cannot be steered by a pilot from the ground to a desired location, as a result the important data can be missed.

Using the radiosonde method means that scientists will experience a gap in data collection. This missed data can be gathered by meteorological UAV combined with the dropsonde system. UAV allows meteorologists to receive data and measurements in real-time. Also, an Air-deployed UAV can be deployed directly into a hazardous storm cloud at a relatively low cost and eliminate the risk to the pilot of the aircraft. Although the radiosonde system still plays an important role when it comes to gathering weather data, using UAV dropsonde is more effective at lower layers of the atmosphere.

Another issue is that radiosondes gather weather data mostly in 10-12 km altitude above the ground. The majority of weather phenomena develop in lower levels of the atmosphere [10] at about 2-3 km from the ground surface. Using Air-deployed UAV allows meteorologists analyse the low altitude areas.

1.1.2. Meteorological radar systems

Weather radars are used to detect the concentration of water droplets and the derivation of rain falling rates within the cloud. The modern weather radars (Fig. 3) are based on a pulse-Doppler system [11, 12], that in addition to providing the rate of precipitation, also estimates the motion of droplet in accordance with the radar and, as a result, can evaluate the radial speed of the cloud movement. The development of dual-polarized weather radar enables a more accurate description of precipitation types and sizes.

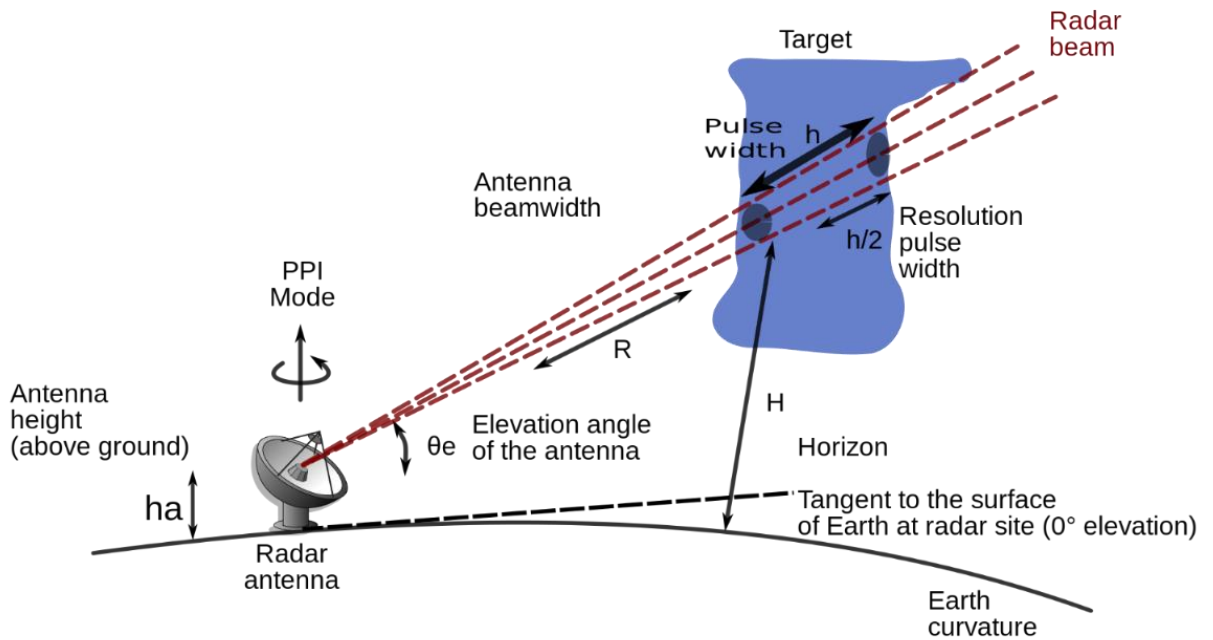


Fig. 3. The radar beam path with respect to height [13]

The radar system measures the lower layer of the atmosphere, nevertheless, the radar antenna is fixed to the ground and cannot be transferred to the different locations and investigate a specific area of the storm cloud. The principal of the radar system analyses only specific parameters of the cloud, in comparison Air-deployed UAV can propose deeper more specific analysis, and gathered data is more accurate.

1.1.3. Weather Satellite systems

The weather satellites are based on visual images of the atmosphere from above, including clouds formations in real-time. These images are very important for weather forecasting; it provides an overview of the whole weather situation covering the Earth surface. There are many applications of the satellite observations, such as weather forecasting, climate change variation detection and atmospheric research [14]. With the development of the sensor's resolution, satellite observation continues improving.

In Figure 4 the space-based observation system is demonstrated. Space-based observation mostly involves low Earth orbit satellites that gather important information to numerical modelling. According to the researchers [4, 15], the constellation of operational geostationary weather satellites remains the foundation of near-surface observations of the meteorological condition. Collected imagery information is produced on an operational basis with data from GOES-West and GOES-East

(NOAA, USA), Meteosat, and Meteosat/IODC (EUMETSAT) and MTSAT (JMA, Japan) [15]. The purpose of supplementary satellites such as the FY-2 series (CMA, China) is to ensure the strength of the system and support the operational stability.

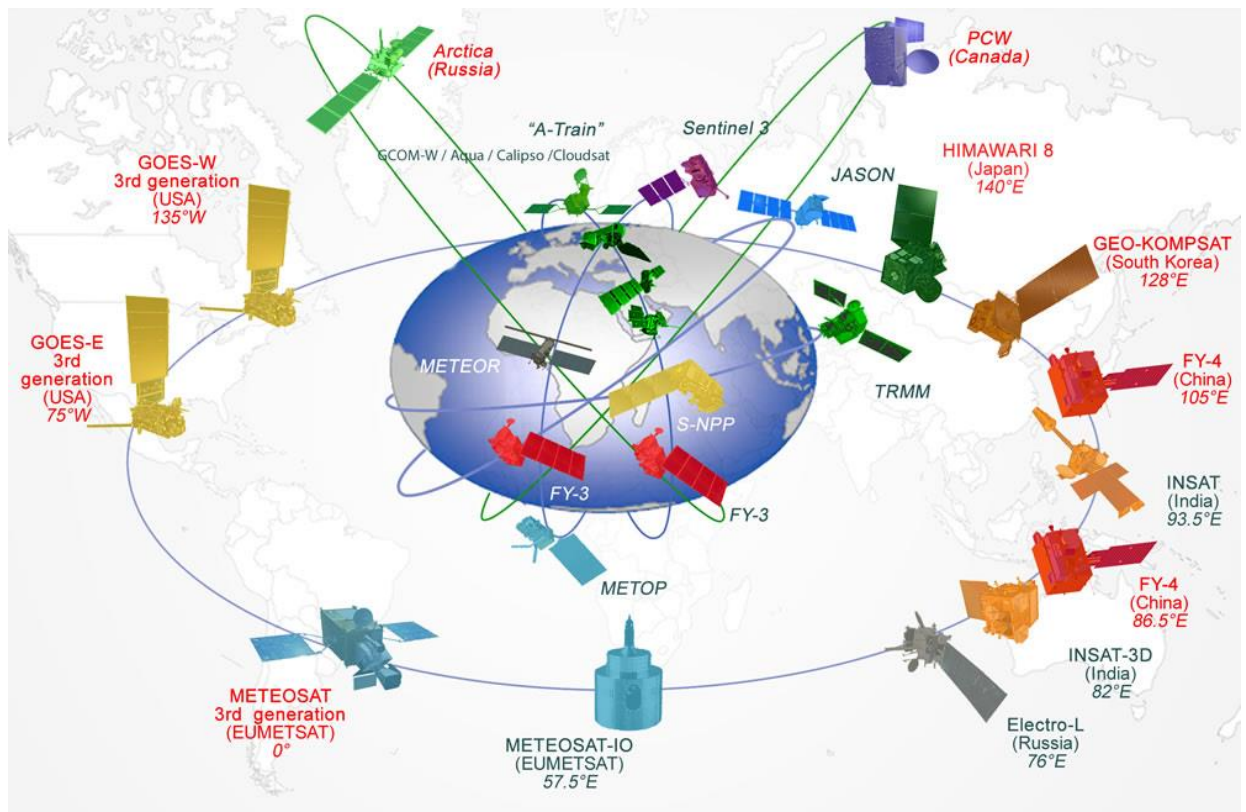


Fig. 4. Space-based observation system [4]

The space-based observations are not suitable for weather information gathering. Although it has a significant impact on weather forecasting, this system is limited in providing detailed information directly from the storm cloud. Even the smallest changes in lower layers of the atmosphere can be essential for storm formation and depending only on satellite imagery are not sufficient. The base principals of the space-based observations

1.1.4. Aircraft-based observations

Aircraft-based observations mostly gather data in the middle layers of the atmosphere. The significant amount of flights allows gathered continuous flow of data. This network is very important not only for the aviation community, but for the global weather observation system as well.

The initial structure of aircraft-based observations was limited to short messages from pilots (PIREP) [16, 17], consisting of little more than radio communications between the pilots and the ground station regarding weather phenomena and conditions received during flight. The development of the systems led to the automated aircraft-based reports (AIREPS) of gathered data while flying such as temperature, humidity, wind speed, and direction in accordance to the position of the aircraft. The International Civil Aviation Organization (ICAO) together with WMO created regulation standards for these reports.

Nowadays, the use of the aircraft based systems for the automated collection of meteorological data has been significantly improved and developed to provide more precise, more timely and, most

importantly a much greater volume of middle-air data in support of data users and meteorological applications [18], including support for weather-related forecasting and monitoring for the aviation community.

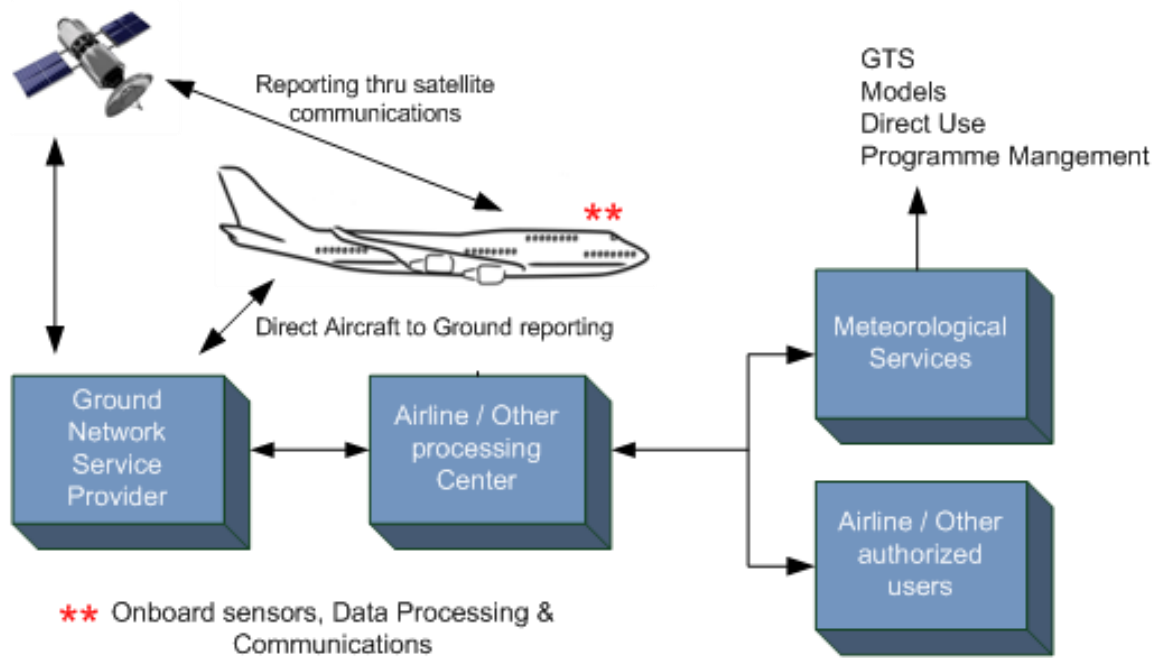


Fig. 5. Aircraft-based observations [18]

Aircraft-based observation is only the additional mission of the aircraft. The reports made from the aircraft are not contributed to the desired location; it only observes weather along the path of the aircraft destination. From this point of view Air-deployed UAV contributes to its mission to gather data in a specific area with no limits of time.

1.1.5. Unmanned Aerial Vehicles

According to the authors in works [19-21] there is a wide area of UAV usage for meteorological researches, to adapt to rapidly changing variables new systems are developed. Fully autonomous mini UAVs are being developed [19] for the weather analysis. UAV with artificial intelligence (AI) is also considered when talking about the improvement of forecasting methods [20], the aircraft that collects the required information from the meteorological database, while still airborne, and makes decisions respectively.

There are a huge variety of developed UAV depending on the mission. The unmanned aircraft such as drones can loiter in the required location, but it is unsafe to send it to the storm cloud, because the system can be damaged irreparably [9]. It can serve for Air-deployed UAV as a carrier, combining both systems significant results can be achieved. The UAV is controlled from the ground station and it always must contain the eyesight with the pilot for the safe retrieval. Most data gathered by UAV are image related, carrying, and deploying dropsondes with the meteorological sensors could expand the abilities of such weather observations.

1.1.6. Air-deployed UAV

The carrier is loaded with individual sensors and then they fly above the storm clouds and the sensors are released to collect meteorological data. These sensors also called dropsondes are designed mostly with small parachutes, which mean that they can collect data as they fall. This method led to develop the research of storm profiles, which was difficult to achieve with other weather observation systems.

The internal components scheme of Vaisala weather data gathering instrument [22] is represented in Figure 6. The principal of the dropsonde is while deployed from a tube in the of weather research aircraft and falling freely through the storm cloud. During its descent, the instrument gathers data such as the temperature, humidity, pressure, wind speed and direction.

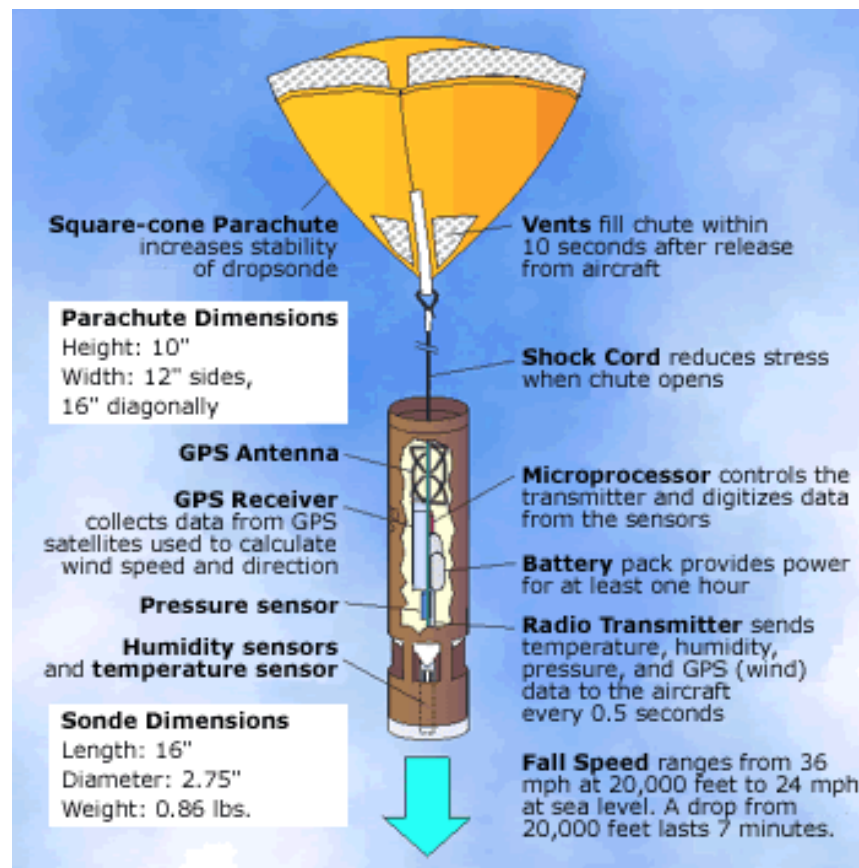


Fig. 6. NCAR/Vaisala dropsonde [22]

The oceanologists are also developing a drifter [23] that will be capable of collecting positional coordinates and transmitting coordinates to a communications satellite. Current drifters are bulky which limits deployment methods to large vessels and are not cost-efficient.

Although this system is being used for a while, it can be improved by providing the data in real-time to the aircraft or the ground station. To reduce flow field disturbance and achieve slow falling velocity in a hazardous weather environment the body of the dropsonde must be investigated.

1.2. Analysis of meteorological systems

Table 1 shows six systems used by GOS for weather observations are compared in accordance with observation altitude, mobility (ability to change the initial position of the observations), controllability (ability to control by a pilot), and system of the safety. According to comparison the

best system to evaluate the signal propagation model in hazardous weather conditions is air-deployed UAV. It analyses low altitudes of the atmosphere; the position of the system is not fixed to the ground station; with the help of other systems, such as other UAV or aircraft it can be deployed in the required position and directly to the storm cloud; relatively inexpensive construction does not require to be retrieved all deployed systems after the weather observation mission, in this context the safety of the system is not applicable.

Table 1. Comparison of weather system

Observation system	Observation altitude	Mobility	Controllability	System safety
Radiosonde	High layers	Non-fixed position	Uncontrollable	Safe
Weather radar	Low layers	Fixed position	Uncontrollable	Safe
Weather satellite	High layers	Fixed position	Uncontrollable	Safe
Aircraft-based	High layers	Non-fixed position	Controllable	Unsafe
Air-deployed UAV	Low layers	Non-fixed position	Controllable	Safe
UAV	Low layers	Non-fixed position	Controllable	Unsafe

Figure 7 represents air-deployed UAV system, combining with the weather balloon, the aircraft, or the UAV the dropsonde is released directly to the storm cloud, the ground station receives data in real-time, during this process the profile of storm cloud can be observed. Some of the dropsondes will drift with the wind identifying the movement of storm gathering essential data required to the weather predictions.

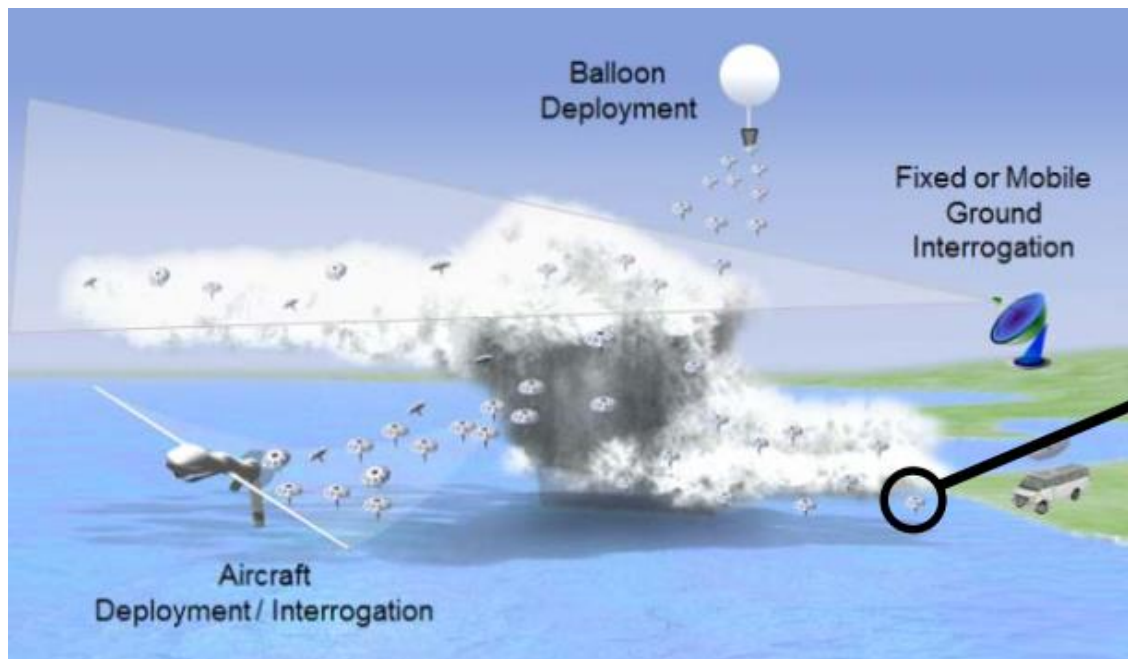


Fig. 7. Air-deployed UAV system [24]

2. The effect of the shape on the falling object

For further analysis, the dropsondes will be used to analyse the signal propagation in normal and hazardous weather conditions. This metrological gathering data method is safer compared to the others, gathers data in the lower layers of the atmosphere, as well, is more cost-efficient. For meteorological sensors to gather the data using dropsonde most important factors are low falling velocity and low flow field disturbance. The purpose is to create light-weighted, simplified dropsonde to gather data at the low level of the atmosphere. These systems are based on falling, the great impact depends on the sensors carrying shape of the body.

2.1. The motion of free-falling objects

The free-falling object is determined as a motion of the body under the influence of gravitational force, described as the weight of the object [25, 26]. The body that moves only because of the action of gravity is said to be free-falling, and in a vacuum accelerates at a constant rate. Its motion is described by Newton's second law of motion, described by the equation (1):

$$m \frac{dv}{dt} = F . \quad (1)$$

The acceleration is constant and equal to the gravitational acceleration g which is approximately 9.81 meters per square second at the sea level. In this case the weight, size, and shape of the object are not a factor in describing a free-fall. Ignoring air resistance, for an object falling close to the earth's surface the force is equation is: $F = mg$, directed downward. Then, the differential equation (2):

$$m \frac{dv}{dt} = mg . \quad (2)$$

This is a mathematical model corresponding to a falling object. The velocity v is an inverse derivative of the constant g ; then $v = gt + C$, where C is a random number. If it is assumed that the initial position of the object, at time $t = 0$, is $y(0) = y_0$, then the displacement of the object is described by equation (3):

$$y = -\frac{1}{2}gt^2 + v_0t + y_0 . \quad (3)$$

2.2. Forces acting on a falling object

As it is known, the force of air resistance is acting oppositely to the direction of the object's motion, with mass proportional to the square of the velocity. Air resistance is equal to kv^2 , where the constant of proportionality k is the determination of the drag coefficient. Combining air resistance and gravitational force, the differential equation model (4) is obtained:

$$\frac{dv}{dt} = g - \frac{k}{m}v^2 . \quad (4)$$

The differential equations describing the velocity of a falling object, described above, were first order. In the related second order equation, $y'' = g$, the unknown function represented by the variable y is the distance which the object has fallen [27]. Then the velocity is $v=y'$. Including air resistance, we get $y'' = g - k(y')^2/m$, another second order equation.

The gravitational acceleration decreases with the square of the distance from the center of the earth. But for most practical problems in the atmosphere, we assume this factor is constant. If the object were falling in a vacuum, this would be the only force acting on the object. But in the atmosphere, the opposing force to the motion of a falling object is the aerodynamic drag. The drag equation (5) shows that drag D is equal to a drag coefficient C_D times one half the air density ρ times the velocity v squared times a reference area A , which is the main factor describing drag coefficient.

$$D = C_D \frac{1}{2} \rho v^2 A . \quad (5)$$

The drag force D depends on the square of the velocity. As the body accelerates its velocity the drag increases. It shortly reaches a point where the drag is the same as the weight. When drag is equal to weight, there is no external force on the object, and the acceleration becomes equal to zero. The object then falls at a constant velocity as described by Newton's first law of motion. The constant velocity is the terminal velocity.

The motion of any moving object can be described by Newton's second law of motion, force F equals mass m times acceleration a . This force causes the speed of the object to increase, assuming that it is directed downwards. The second force on the object results because the fall occurs in the atmosphere, meaning that there is an air resistance. This tends to slow the object down, and so is in the opposite direction from the gravitational force. Combining both forces we get equation (6).

$$F = mg - \gamma v . \quad (6)$$

It is assumed, that the air resistance force is proportional to the velocity, giving a term $-\gamma v$, where γ is constant. The assumption here is that the distance is moving downward, and so $v > 0$ means the object is falling. The minus sign in the resistance force term is to make sure that this force slows the object downwards. Substituting into Newton's law we receive the equation (7):

$$m \frac{dv}{dt} = mg - \gamma v . \quad (7)$$

The previous equation can be simplified by dividing both side by m (8), resulting:

$$\frac{dv}{dt} = g - \frac{\gamma}{m} v . \quad (8)$$

2.3. The effect of the drag on the shape

An object in a fall condition contributes to a gravitational force which is constant in a viscous fluid, is calculated by a drag which is proportional to its velocity. The drag coefficient depends on drag produced on the shape, shape surface area, inclination, and flow conditions [29]. The drag coefficient C_D in equation (9) is equal to the drag force D divided by the force produced by the dynamic pressure: one half density ρ times squared velocity v , times reference area A .

$$C_D = D / \left(\frac{1}{2} \rho v^2 A \right) . \quad (9)$$

Experimentally the drag coefficient usually is tested by placing the small model of the object into the wind tunnel. The amount of drag is being calculated, including the tunnel environment, velocity, and the reference area of the model. The tunnel use the front surface as the reference area (Fig.8).

To ensure the correct analysis of the shape produced drag, the comparison must use the same reference area of the analysed objects, as well as the equal Reynolds or Mach number, to achieve correct values of the drag coefficient.

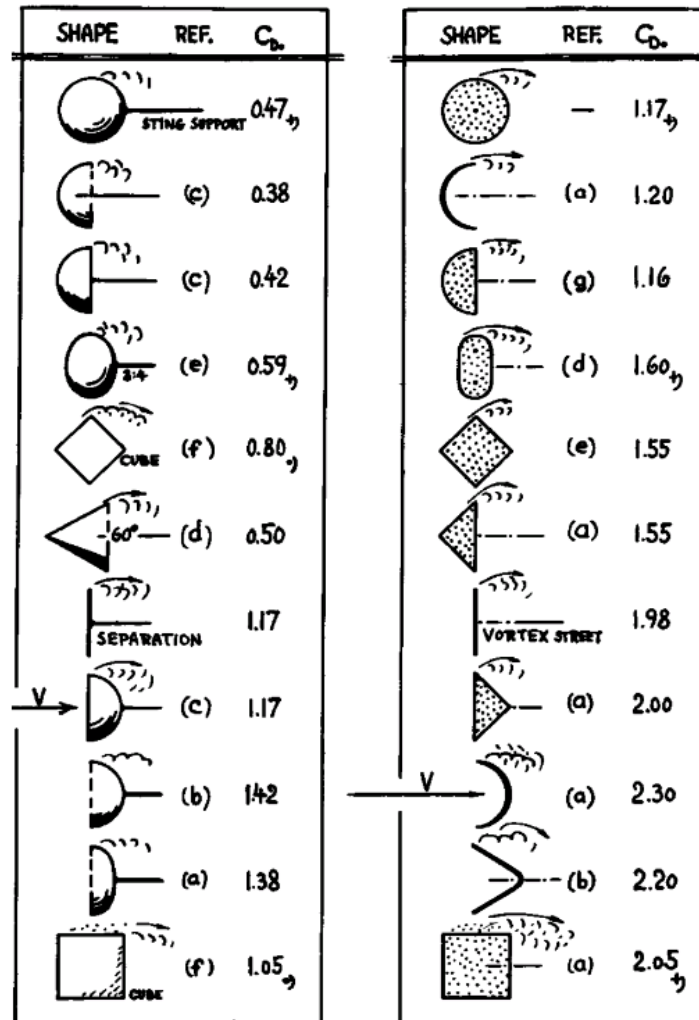


Fig. 8. Drag coefficient according to the shape of the body [29]

The drag coefficient depends on the shape of the object and its attitude. Also, it must be ensured that the viscosity and compressibility effects are the same for all models, as they have great impact on drag Coefficient. In the other way, the accuracy of the prediction will be influenced.

3. The impact of weather phenomena to the UAV signal propagation

3.1. Path losses

Most UAV signal path losses simulations are based on already known models used to model ground-to-ground connections, one of which is the so-called log-normal path losses model [30–37]. According to this model, the distance loss dependence on distance $PL(d)$ is generally described by the equation (10):

$$PL(d) = PL(d_0) + 10n \lg\left(\frac{d}{d_0}\right) + X_\sigma ; \quad (10)$$

where $PL(d)$ is path losses [dB]; $PL(d_0)$ is known path losses at a small distance d_0 (usually about 1 m) from the transmitter; n is a degree indicator which describes the propagation conditions of the signal; X_σ is a so-called shadowing component which describes the influence of various signal propagation mechanisms on signal loss and measurement conditions. Usually, X_σ is expressed as a random variable of a normal distribution with zero first moment and σ second moment, i.e. $X_\sigma \sim N(0, \sigma^2)$. In practical calculations, instead of X_σ , simply σ is used.

Sometimes the formula (10) is slightly changed when constant β is used instead of member $PL(d_0)$ to estimate the number of factors such as antenna gain, polarization, and operating frequency:

$$PL(d) = 10n \lg\left(\frac{d}{d_0}\right) + \beta + X_\sigma . \quad (11)$$

As mentioned above, the grade n evaluates signal propagation conditions: if $n = 2$, we have a standard free-space model when signal losses variations correspond to signal losses variations in free space FSL (12):

$$FSL = 92.45 + 20 \lg(d_{[\text{km}]}) + 20 \lg(f_{[\text{GHz}]}) ; \quad (12)$$

where f is the frequency of the signal carrier.

Various equation (11) modifications are also frequently encountered which apply to one or other specific conditions [34].

If $n > 2$, we have a case where the signal transmits in space with many obstacles, this is when the propagation of the signal is strongly influenced by mechanisms such as diffraction, reflection, scattering, refraction. When $n < 2$, we have a so-called waveguide effect when the signal can propagate further than what is defined by the free space model (12).

The effect of shadowing on the propagation of the signal is expressed as additional noise. In signal theory, noise is measured as white noise and is modelled using a random number generator.

Sometimes, as noted in the works [38, 39], other well-known models of UAV signal modelling can be used: Okumura-Hata, COST231 Hata, Walfisch-Ikegami and others.

Analysis of these works shows that most of them are performed at relatively low altitudes. At these altitudes, the refractive index change does not play a big role. In addition, most of them perform well in good meteorological conditions. Therefore, in practice, it is not a question of how much these simulation results will match real results at higher altitudes even under good meteorological conditions.

3.2. Rain impact

In most of the works the rain impact is assessed using the formulas proposed by ITU-R Recommendation P.838. According to this recommendation, the rain intensity is divided into weak (1.25 mm/h), medium (depending on the zone, Lithuania may be up to 70 mm/h depending on some parameters) and strong (about 150 mm/h) intensity rain and attenuation is evaluated by the formula (13):

$$\gamma = kR^\alpha ; \quad (13)$$

where γ is a specific attenuation [dB/km]; k and α are constants dependent on signal polarization and frequency and are found in special tables; R is rain intensity in mm/h. Rain-affected path losses are calculated by multiplying γ by the distance in which it rains. For frequencies 1 and 2 GHz, the corresponding k and α coefficients for horizontal polarization are $k_{h, 1GHz} = 0.0000387$ and $\alpha_{h, 1GHz} = 0.912$ and $k_{h, 2GHz} = 0.000154$ and $\alpha_{h, 2GHz} = 0.63$.

In some cases, such as broadband wireless networks (BWA), it is proposed to change the constant k and α to a and b respectively [39]:

$$\begin{aligned} \gamma &= aR^b \\ a &= G_a f_{[GHz]}^{Ea}; b = G_b f_{[GHz]}^{Eb}; \end{aligned} \quad (14)$$

where, G_a , G_b , E_a and E_b are depended on the frequencies. If $f < 2.9$ GHz, then

$$G_a = 6.39 \cdot 10^{-5}; E_a = 2.03; G_b = 0.851; E_b = -0.079.$$

As it is known, the rain is distributed unevenly throughout the distance, so using the formula (13) directly results are not accurate. The ITU-R Recommendation P.530 suggests using the concept of effective distance d_{eff} , defined by the following equation (15):

$$d_{eff} = d_{[km]} r \quad (15)$$

where d is the distance between the transmitter and the receiver, and the factor r is calculated as follows (16):

$$r = \frac{1}{\left(1 + \frac{d}{d_0}\right)} \quad (16)$$

and

$$d_0 = \begin{cases} 35 \cdot e^{-0.015 \cdot R} & R < 100 \text{ mm/h} \\ 7.81 & R > 100 \text{ mm/h} \end{cases}$$

R is the rain intensity that exceeds the annual time by more than 0.01%, which is 52.6 mins per year. The value of R is selected by region from special tables. For example, Lithuania belongs to Region E, and R at the 0.01% is 22 mm/h.

3.3. The influence of clouds

The influence of clouds, viewed as an entirety of water droplets, on the propagation of high-frequency waves (> 800 MHz) is considered in works [39-41]. ITU has also made its recommendation P.840-7, which offers a cloud impact assessment model. As noted in the work [40], the spread of radio waves is influenced by clouds that are up to 4 km high.

As noted in the ITU-R Recommendation P.840-7, fog and clouds are, as a rule, made up of droplets with a diameter $d < 0.1$ mm. In this case, the Ray approximation is valid and electromagnetic wave attenuation is described by the formula:

$$\gamma_c(f, T) = K(l, T)M; \quad (17)$$

where T is the temperature [K]; K is the specific inhibition factor $\left[\frac{dB/km}{g/m^3} \right]$, M is the density of liquid water $[g/m^3]$; f is the frequency [GHz].

In other works, there are offered slightly different K and M assessment methods.

In the work [40] it is suggested to evaluate K according to the respective graphs, which show the dependence of K variation on temperature and frequency. This dependency corresponds to the linear variation of K in the logarithmic scale (18):

$$\lg K(f, T) = 1.986 \lg f + b; \quad (18)$$

where the factor b depends on the temperature. M , meanwhile, is found in special maps depending on the region and time when the density exceeds a certain normalized size. In the case of Lithuania, where the time is 10%, the density is $M = 0.2$ kg/m³, and when the time is 1%, then $M = 0.8$ kg/m³.

The work [39] suggests the following evaluation of electromagnetic wave suppression:

$$\gamma_C = \frac{\pi^5 d^6}{\lambda^4} k^2; \quad (19)$$

where d is the diameter of the water droplet and k is the coefficient of dielectric properties of the water droplet and is given by the formula:

$$k^2 = \frac{\varepsilon - 1}{\varepsilon + 2}; \quad (20)$$

where ε is the dielectric cloud forming particle constant. As mentioned above, the diameter of the water droplets is generally 0.1 mm.

At work [41], the density of liquid water is suggested not by special maps but by real thermodynamic parameters using the formula (21):

$$M = \frac{\left(\frac{\rho}{R_\alpha T} \right) (1+x)}{1 + \frac{xR_w}{R_\alpha}}. \quad (21)$$

Where $R_a=286.9 \frac{\text{J}}{\text{kgK}}$ is an air gas constant; $R_w=461.5 \frac{\text{J}}{\text{kgK}}$ is a water vapour gas constant; T is the temperature [K]; x is the specific humidity; ρ is the pressure at that height [Pa].

4. Air-Deployed UAV body analysis

4.1. Shape of the dropsonde evaluation

The purpose of this chapter is to evaluate the shape of the Air-deployed UAV, keeping a balance between low flow field disturbance and low falling velocity. These results will be achieved by using Computational Fluid Dynamics (CFD) numerical analysis, to simulate the flow field of the fluid, and the interaction of the air with the body.

According to the other author research on falling objects fall into two types in general. They either assume objects fall at their terminal velocity [43], or they use several typical Reynolds numbers for the falling situations [47]. For both types, the object position and orientation are fixed in the computational domain and do not change with time.

Several basic geometric shapes were chosen for the analysis (Fig. 9).

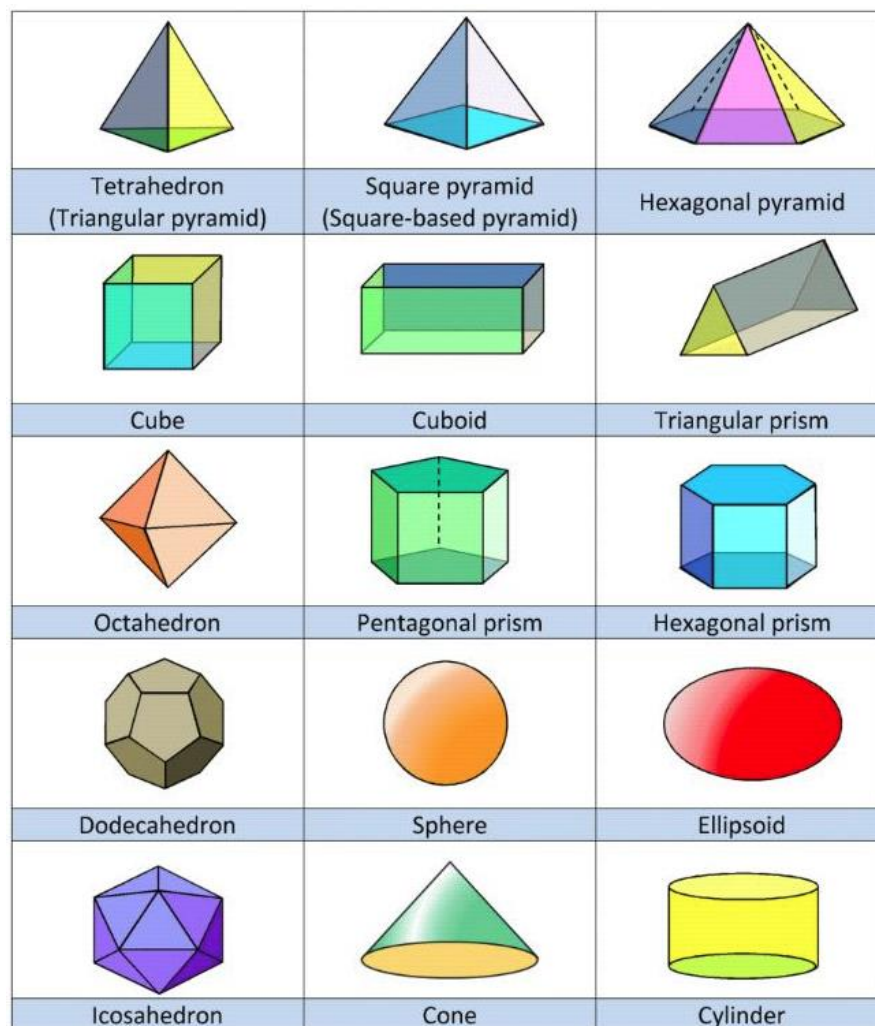


Fig. 9. Geometric shapes for analysis

4.2. Drag coefficient analysis

The shapes were tested using Solidworks Flow Simulation analysis [42]. The same surface area was 0.016 m^2 , Reynolds number was set to 8000 and velocity 3 m/s^2 . Air density 1.204 kg/m^3 .

The results obtained are represented in ascending order in Table 2. The least drag coefficient was achieved with the triangular prism ($C_D = 0.04$), and the least – with hexagonal pyramid ($C_D = 0.36$).

It is noticed that the features of the shape have a great influence on the Drag Coefficient. The flatter the body the higher Drag Coefficient and opposite the narrower – the lower. The shapes with the pointed edges produce less flow field disturbance, the as well as the symmetrical shapes.

Table 2. Coefficient of Drag of the shapes




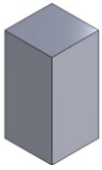









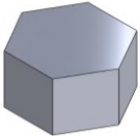
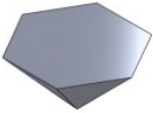
Image of the shape	Shape name	The features of the shape	Coefficient of Drag
	Triangular prism	Narrow, long body	0.044108642
	Ellipsoid	Smooth, long body	0.054443094
	Sphere	Round, symmetrical, smooth	0.065931986
	Cuboid	Narrow, long body	0.084394573
	Tetrahedron	Pointed edge	0.09091106
	Dodecahedron	Round, rough surface	0.129383454
	Cone	Pointed edge	0.131162983
	Octahedron	Symmetrical, pointed edge	0.133353361
	Icosahedron	Round, rough surface	0.136260388

Image of the shape	Shape name	The features of the shape	Coefficient of Drag
	Square pyramid	Pointed edge	0.139970181
	Cylinder	Long body	0.164417736
	Cube	Symmetrical	0.174156813
	Pentagonal prism	Flat body	0.209923364
	Hexagonal prism	Flat body	0.243880462
	Hexagonal pyramid	Very wide, flat body, pointed edge	0.358412063

We will use the shape of the octahedron in the next steps of the research. This figure has coefficient of drag equal to 0.13. It is not the largest C_D , but the body of octahedron has the features effecting the fall velocity and helps to distribute the field flow around the body, this is expected to reduce rotation during falling state.

Further analysis will include additional elements to the construction, such as streamer tail, parachute, and turbine wings. These elements were chosen to eliminate rotating motion of the body and slow down the falling velocity.

4.3. Additional elements for slower descent

To stabilise the descent directional attitude additional elements for UAV body were tested using Solidworks Flow simulation the Computation Fluids dynamics tool. This method allows to predict fluid flow field behaviour within the limits set in a computational domain.

The parachute, streamer tail, and turbine wings were added, to achieve more attitude-stable descent. The analysis eliminates the factor of the material parameters including flexibility and depends only on the shape.

The velocity, side velocity, and vorticity were tested during analysis. For velocity measurement in according to the Y axe the falling speed was set to 3 m/s; side velocity was set cording to 3 axes: X

– 2 m/s, Y – 3 m/s and Z – 1 m/s. The same parameters were used for vorticity analysis of the fluid flow field.

The object in this research is not assumed stationary at the beginning. Rather, it has been falling at a reference velocity close to its terminal velocity. This setup shortens the distance through which an object must travel to reach a steady-state, which is the focus of this research. It reduces both the number of time steps and the computational domain size and, accordingly, improves the computational efficiency.

In figure 10 the initial velocity of the flow field of octahedron is represented in XY axes. It varies from 3.310 to –0.995 m/s. The results show that the shape has influenced the stream velocity negatively. The computed flow field is quite narrow and laminar. The flow field disturbance is laminar, there is no significant impact of the turbulence.

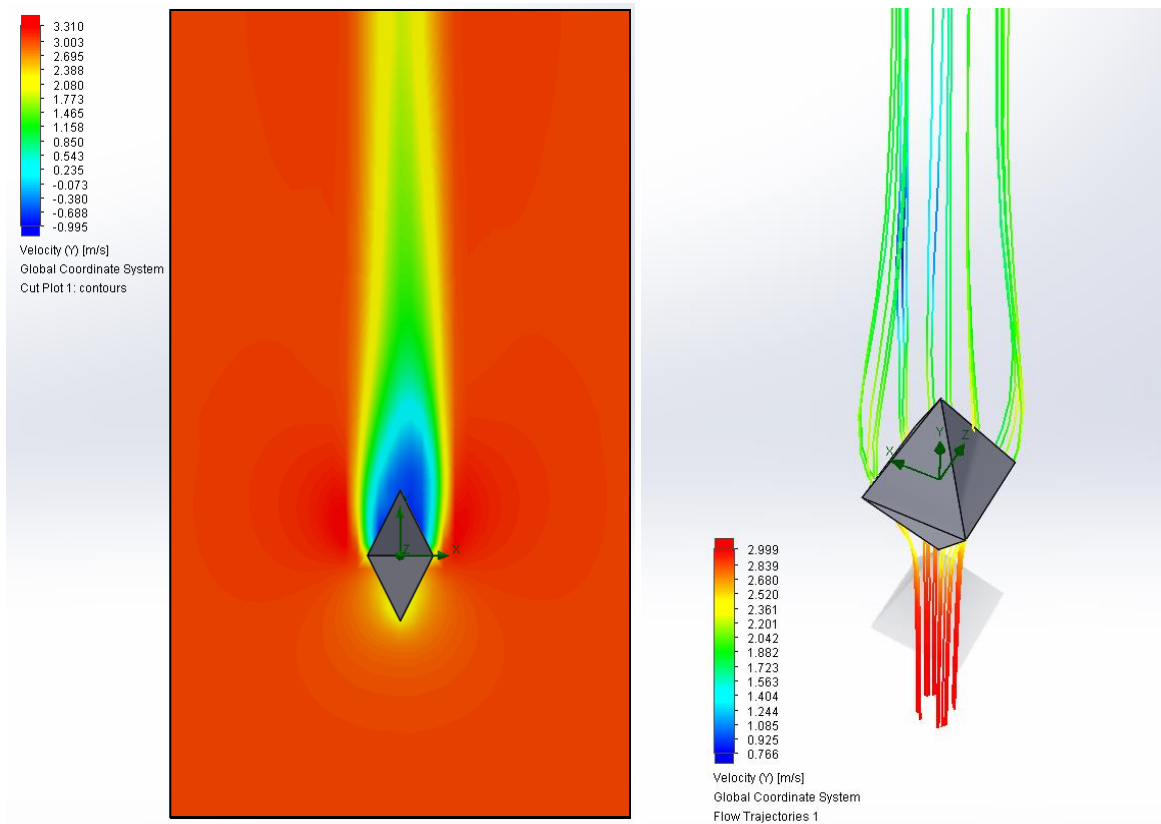


Fig. 10. Velocity profiles of octahedron

Figures 11-13 demonstrates the profile of octahedron with additional gadgets. From Y direction velocity in Figure 11 it is seen that all gadgets help to slow down the flow velocity around the falling object. Parachute was created in the shape of “X” this helps to reduce the effect of distraction in a storm environment. The flow distributes widely around the parachute, also slowing the stream quite effectively.

The streamer tail has a smaller influence on stream disturbance and still slows down the flow field.

The turbine wings also distribute the flow broadly, but the stream velocity is affected slightly. It seems that the turbine wings have a minimum influence on the dropsonde performance, from the results we can see that the falling velocity is affected even contrary than expected, from 3.134 m/s to 1.055 m/s.

The side flow analysis shown in Figure 12 demonstrates the parachute disturbs the flow mostly and the turbine wings – the least. The flow field distributes quite equally around the streamer tail.

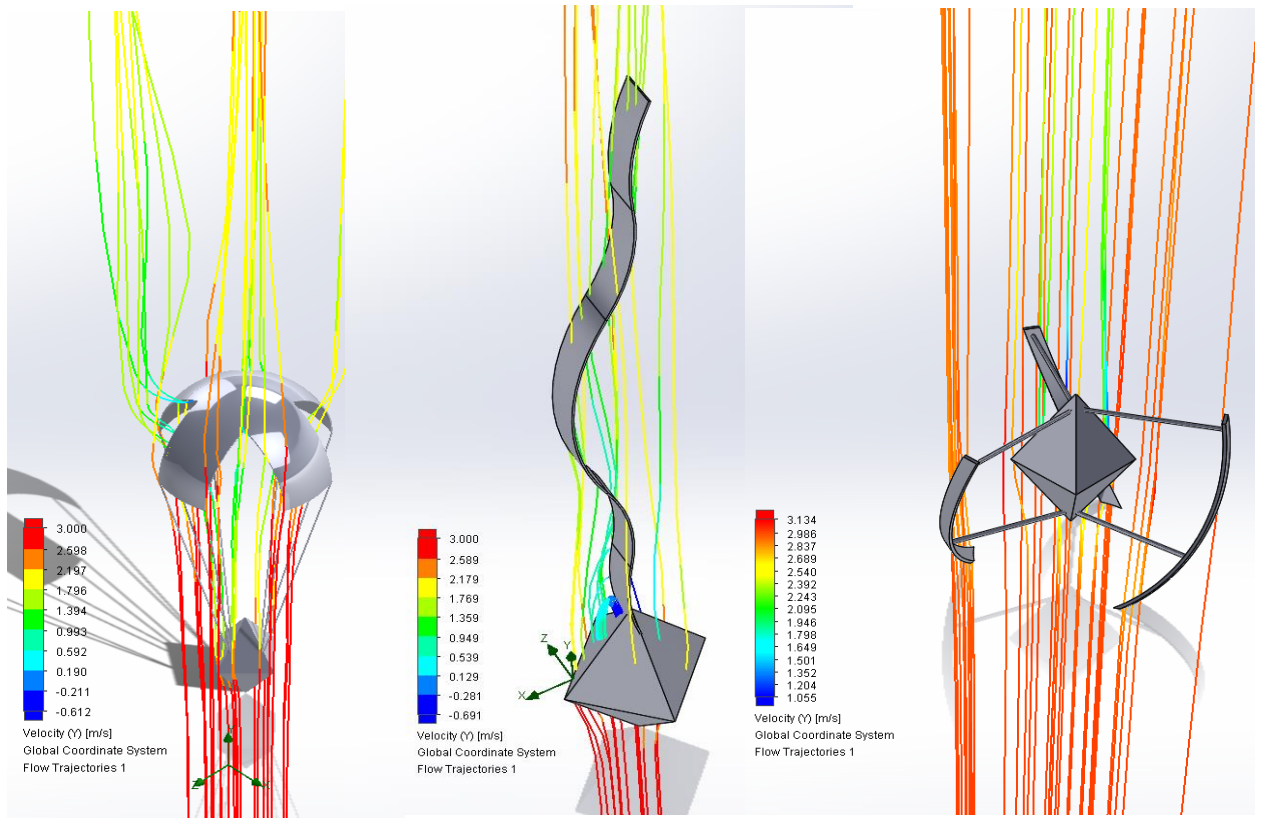


Fig. 11. From left to right parachute, streamer, turbine wings. One directional steady flow.

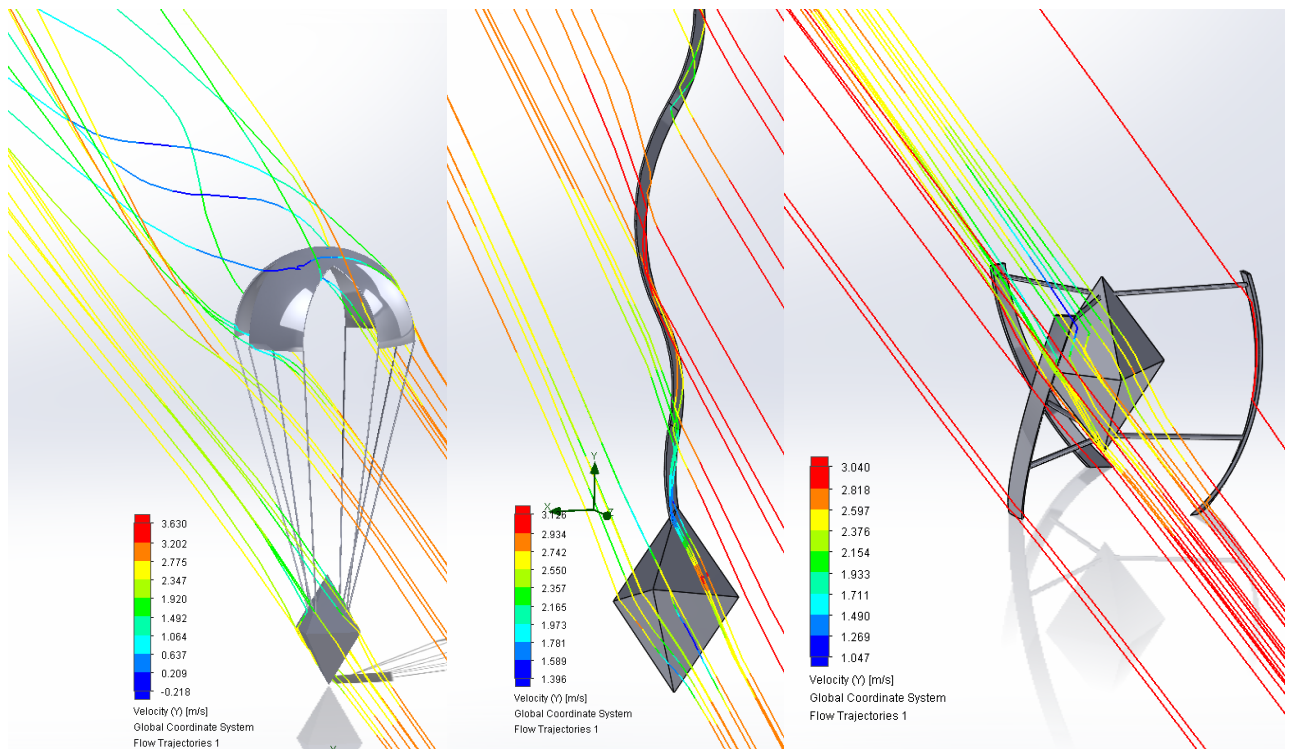


Fig. 12. From left to right parachute, streamer, and turbine wings. Side flow of the stream.

The very similar results were achieved with vorticity analysis represented in Figure 13. Parachute vorticity maximum factor is equal to 108.12 per second which is the largest, streamer – 96.95 per second, and turbine wings – 54.91 per second.

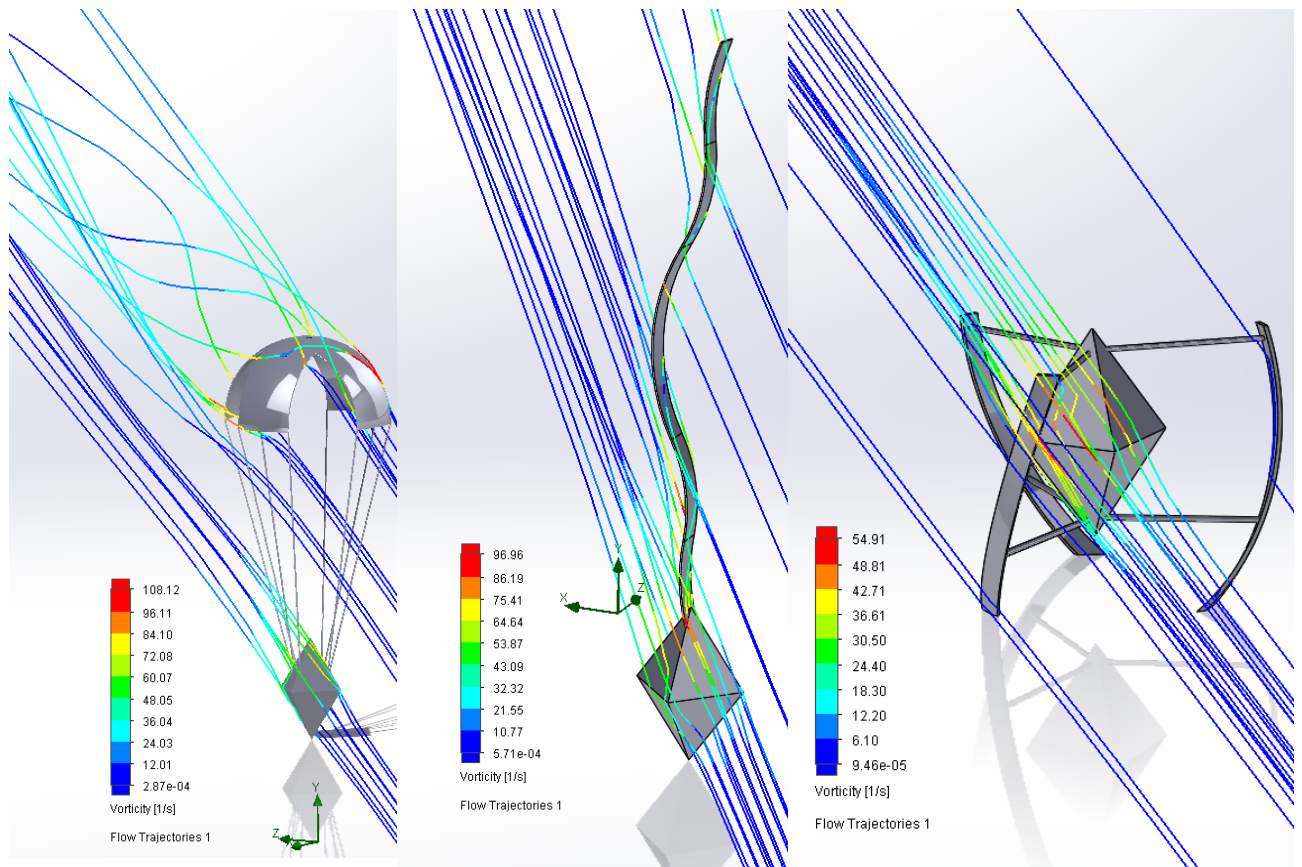


Fig. 13. From left to right parachute, streamer, and turbine wings. Side-stream Vorticity.

The analysis revealed that the turbine wings achieved negative results. From the two options left the better performance demonstrated streamer tail, than the parachute. It helped to reduce the flow velocity, before the streamer tail was added the results was from 3.310 to -0.995 m/s, and after from 3.00 m/s to -0.691 m/s.

5. UAV signal propagation simulation

5.1. Stochastic equations

In general, a signal is understood as a physical process in which information is transmitted in time and space. The signal has two components: deterministic and random. In general, the signal is described by the following stochastic differential equation:

$$dX_t = a(X_t, t)dt + \sum_k b(X_{t_k}, t_k)dW_i; \quad (22)$$

where X_t is a stochastic process, $a(\cdot)$ is a determinative component of the stochastic process and is called a "drift", showing how much the initial X value changes with each subsequent step, $b(\cdot)$ is the dispersion indicating the statistical nature of the signal, and W_i defines the signal noise characteristics and is called the Wiener process.

This equation can be presented in various forms, depending on the tasks being solved. In the final differential form, consider t_1, t_2, \dots, t_k . If we look at the discrete signal variation (at small-time moments Δt), then the signal level X_i will depend on the previous signal level X_{i-1} :

$$x_i = x_{i-1} + a_i \Delta t + b_i (W_k - W_{k-1}) \Delta t; \quad (23)$$

then this equation can be written as follows:

$$X_k = X_0 + \sum_{i=1}^k a_i \Delta t_i + \sum_{i=1}^k b_i \Delta W_i. \quad (24)$$

In case when $\Delta t \rightarrow 0$, we get:

$$X_t = X_0 + \int_0^t a(X_t, t)dt + \int_0^t b(X_t, t)dW_t. \quad (25)$$

In this equation, the first member X_0 represents the initial value of the process. In terms of signal loss in space, it would be the losses in free space. The second member $a(\cdot)$ describes the shadowing effects that increase the signal propagation loss in terms of losses in free space. The third member $b(\cdot) dW_t$ describes the noise that appears as the scattering of the data in the signal envelope. In general, the Wiener process corresponds to the probability density distribution, usually as normal, $dW \sim N(\mu, \sigma)$, where μ is an average and equal 0 in the calculations, and σ is the dispersion and is usually taken in the calculations as 1 [44, 45]. In that case, we have a so-called white noise.

Equation (25), depending on the distribution that describes the process, will have a different stochastic differential equation.

Depending on the distribution that best describes the process and considering (22) and (25), we will have different forms of such a stochastic differential equation. If the process corresponds to a normal distribution, then the corresponding stochastic differential equation will be:

$$dX = X_0 - \frac{\varepsilon}{2\sigma^2} X(t) \text{sign}(X) dt + \sigma W(t) dt; \quad (26)$$

where ε is a freely selectable parameter.

If the process corresponds to the log-normal distribution, then the corresponding stochastic differential equation will be as follows:

$$dX = X_0 - \varepsilon X(t) \left(\ln \left(\frac{X(t)}{\mu} \right) - \sigma^2 \right) dt + \varepsilon X(t) W(t) dt . \quad (27)$$

Since, as mentioned above, the signal is the process changing in time and space, we can solve these equations separately, both in time and in space, only in this case we change the time difference dt into the distance differential ds . Let's assume that the propagation of the signal is influenced only by slow decay, which is characterized by normal distribution. Then the equation (26) would look like this:

$$dPL = FSL - \frac{\varepsilon}{2\sigma^2} \Delta PL(s) \text{sign}(\Delta PL(s)) ds + \sigma \xi(s) ds ; \quad (28)$$

where PL is signal losses at the calculated point; FSL is Free Space Losses, expressed in equation (24); σ is the standard deviation for shadowing effect; ξ is standard deviation defining the process of the Wiener; ε is freely selectable member; $\Delta PL(s) = PL(s) - FSL$.

5.2. Path losses

To propose a signal propagation model based on equation (28), this equation needs to be integrated. This is possible if we know the change of $PL(s)$. Since in the works [30–37] the signal variation is examined at relatively low altitudes (usually up to 500 m), we assume that the established patterns are also valid at higher altitudes, bearing in mind that these works do not question the accuracy of the shadowing effect model (23).

The results of works [2, 3, 30, 33] with extrapolation to heights up to 5000 are shown in Figure 14. As we can see, the results of even small altitudes [30] are noticeable, but this is explained by the fact that measurements were carried out over the sea, which has a particularly good reflection coefficient, and which causes the loss to increase significantly. Meanwhile, the results [2, 3, 33] coincide quite well even though experiments were performed at different frequencies ($f \sim 800$ MHz [2,3] and 2.45 GHz [33]). Path losses by works [32] and [33] can be described by equation (23) with the corresponding coefficients: $\beta = 48.8$ dB; $n = 1.9$ and $\sigma = 5.2$ dB for work [32] and $\beta = 48.4$ dB; $n = 1.759$ and $\sigma = 3.8$ dB for operation [33]. Therefore, the following data will be used to develop the stochastic model: when the frequency of the signal is 810 MHz, the equation (23) parameters defined in the work [32] are used, and when the frequency is 2.45 GHz will be used the parameters of work [36]:

$$PL_{810} = 10 \cdot 1.9 \lg(s) + 48.8 + 5.2 = 19 \lg(s) + 54 ; \quad (29)$$

$$PL_{2.45} = 10 \cdot 1.75 \cdot \lg(s) + 48.4 + 3.2 = 17.5 \lg(s) + 51.6. \quad (30)$$

It should be considered that the above-mentioned works have been performed under good weather conditions and do not consider the influence of rain or clouds. Rain and clouds have a significant impact on path losses. In hazardous atmospheric conditions (rain intensity $R = 150$ mm/h and liquid water density $M = 800$ g/m³), the variation of the path losses is shown in Figure 15.

As can be seen, under hazardous atmospheric conditions, the variation of the path losses does not correspond to the model (22), so it is appropriate to use other models to predict the loss of path losses.

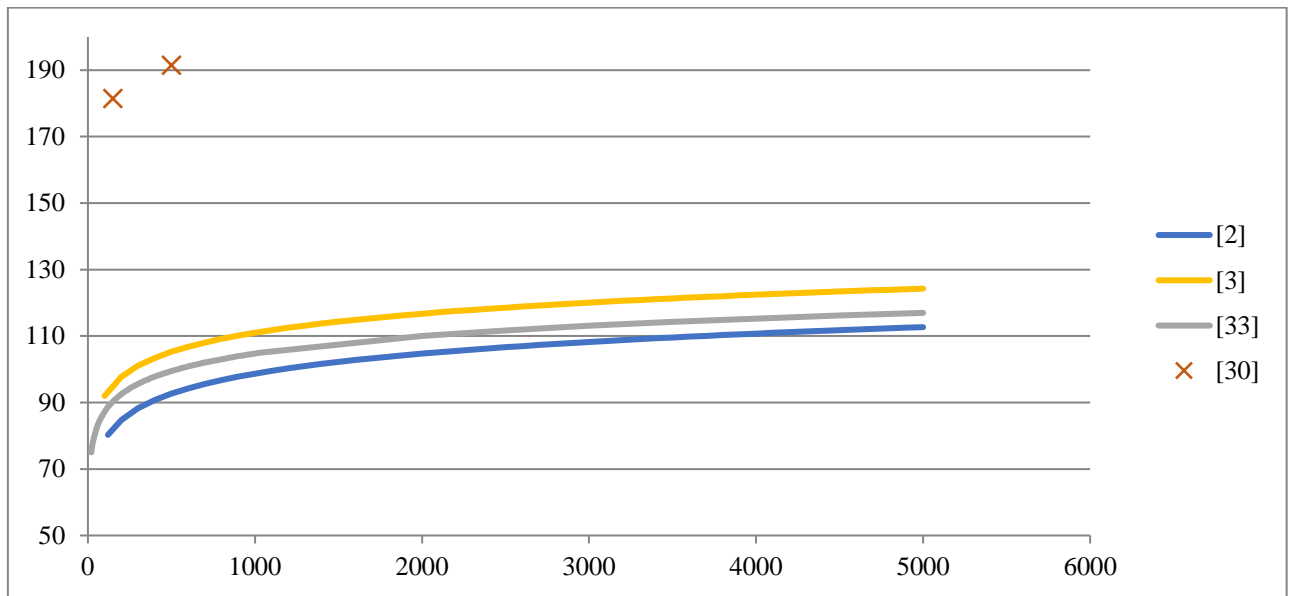


Fig. 14. PL extrapolation to height (h), according to works [2], [3], [30] and [33]

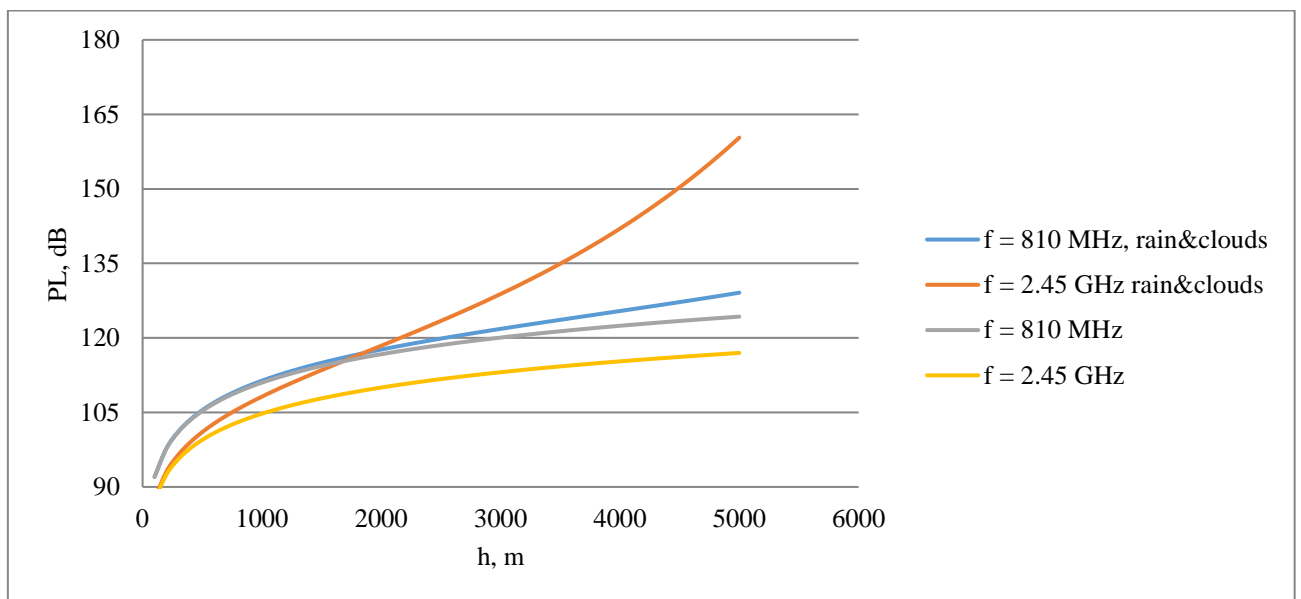


Fig. 15. Variation of the path losses in hazardous weather conditions

The higher the frequency, the greater the deviation from the (22) model, and this deviation begins to feel about 400 m high. For the lower frequency ($f = 810$ MHz) the deviation from (22) is observed from around 2000 m.

Such high losses at frequency $f = 2.45$ GHz mean that data exchange in real-time under hazardous atmospheric conditions for altitudes above 2000 m is practically impossible. This is because the sensitivity of the receivers working in this frequency is in most cases not lower than -95 dBm, and the threshold of the best receivers is not lower -110 dBm.

Nevertheless, this work creates a model for both at the 810 MHz and 2.45 GHz bands.

5.3. Evaluation of the Wiener process

To estimate white noise the standard deviations for white noises $\sigma_{wn} = 0.5; 1; 2$ was modelled at this work (Fig. 16).

As it is seen, as the distance from the transmitter increases, these noise increases and have a greater impact on the signal. At higher noise levels, the signal may be heavily distorted or even not detected at all.

Further simulations will use three types of Wiener processes, with $\zeta = 0.5$ and 1, and a standard deviation that corresponds to the selected standard deviation of the shadowing effect $\zeta = \sigma$.

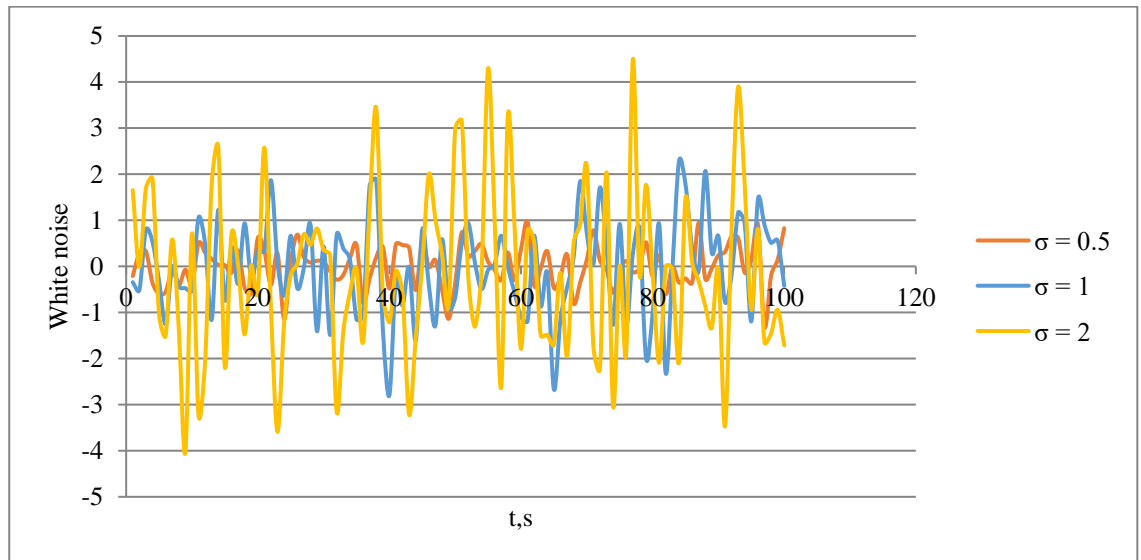


Fig. 16. Standard deviations for white noises model

This noise in terms of path losses (18) is illustrated in Figure 17.

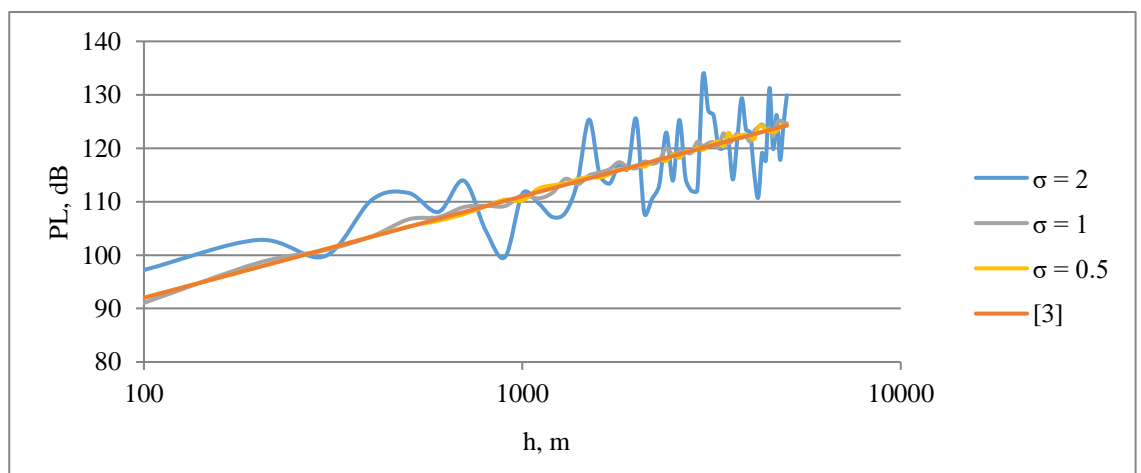


Fig. 17. Noise in terms of path losses

5.4. The influence of the Rain

The influence of rain is evaluated according to formula (25). It should be taken into account that the ITU-R recommendation P.838 only contains data for frequencies $f \geq 1$ GHz. Therefore, it is assumed in our work that rain attenuation at frequencies 810 MHz will be very similar to attenuation at 1 GHz.

In addition, the calculations will be carried out under intense rain conditions, when rain intensity in the Lithuanian zone (zone E) is 150 mm/h.

5.5. The influence of clouds

As already mentioned, the influence of clouds on signal attenuation is defined by (17) equation. Knowing that in the troposphere the temperature T increases by the height h linearly by the formula:

$$T_{[^{\circ}C]} = -6.5h_{[m]} + 15; \quad (31)$$

and according to the variation of specific inhibition factor K given in [40], it is possible to determine the regularity of variation of the coefficient b in formula (18).

The coefficient b in the frequency range from 900 MHz to 3 GHz is well approximated by the formula:

$$b = 0.0001 \cdot (-6.5h_{[m]} + 15)^2 - 0.0146 \cdot (-6.5h_{[m]} + 15) - 3.0254. \quad (32)$$

Thus, in general, the specific attenuation factor can be expressed as:

$$(33)$$

$$\lg K(f, T) = 1.9861 \lg f - b = 1.9861 \lg f + 0.0001 \cdot (-6.5h_{[m]} + 15)^2 - 0.0146(-6.5h_{[m]} + 15) - 3.0254;$$

or

$$K = 10^{1.9861 \lg f + 0.0001 \cdot (-6.5h_{[m]} + 15)^2 - 0.0146(-6.5h_{[m]} + 15) - 3.0254}. \quad (34)$$

The total path loss due to clouds in the PL_c will be:

$$PL_c = K \cdot d_c; \quad (35)$$

where d_c is the thickness of the cloud, km.

The model assumes that the cloud thickness $d_c = 1$ km.

5.6. Signal propagation PL predicting model

The model was created with the following parameters (Table 3):

Table 3. Model parameters

Frequency	810 MHz				2.45 GHz			
σ , dB	2	3.8	5.2	6.2	2	3.8	5.2	6.2
ξ , dB	0.5	0.5	0.5	0.5	0.5	0.5	0.5	0.5
	1	1	1	1	1	1	1	1
	2	3.8	5.2	6.2	2	3.8	5.2	6.2

With these data set into (18), (19) and (14) and integrated we get:

$$PL_{810} = FSL + \frac{\varepsilon}{\sigma^2} s(0.4985lg(s) - 11.9065) + \sigma\zeta s + \frac{\varepsilon}{4\sigma^2} \left(\frac{s}{1000}\right) (\gamma_{rain} + \gamma_{cloud}) \quad (36)$$

$$PL_{2.45} = FSL + \frac{\varepsilon}{\sigma^2} s(1.48595lg(s) - 6.0036) + \sigma\zeta s + \frac{\varepsilon}{4\sigma^2} \left(\frac{s}{1000}\right) (\gamma_{rain} + \gamma_{cloud}) \quad (37)$$

As already mentioned, ε is a freely elective member. The selection of the numerical value of this member makes it practically ideal to model the path losses variations with respect to preliminary calculations. The error is $< 1\%$. However, it should be noted that these losses of the path are very sensitive to the change of ε .

5.7. The measurement of the path losses

The experiment was performed in normal weather conditions (temperature 19°C, humidity 1016 hPa), using DJI Phantom 4 model drone in 2.45 GHz frequency, power transmitted $P_{TX} = 17\text{dBm}$, height achieved 450 m vertically.

Figure 18 demonstrates the measurement results compared to the created model. Calculated PL from the measurement distributes along the 2.45 GHz curve, but there is no significant difference between normal and hazardous conditions, this is because the model difference increase from about 2000 m above the ground.

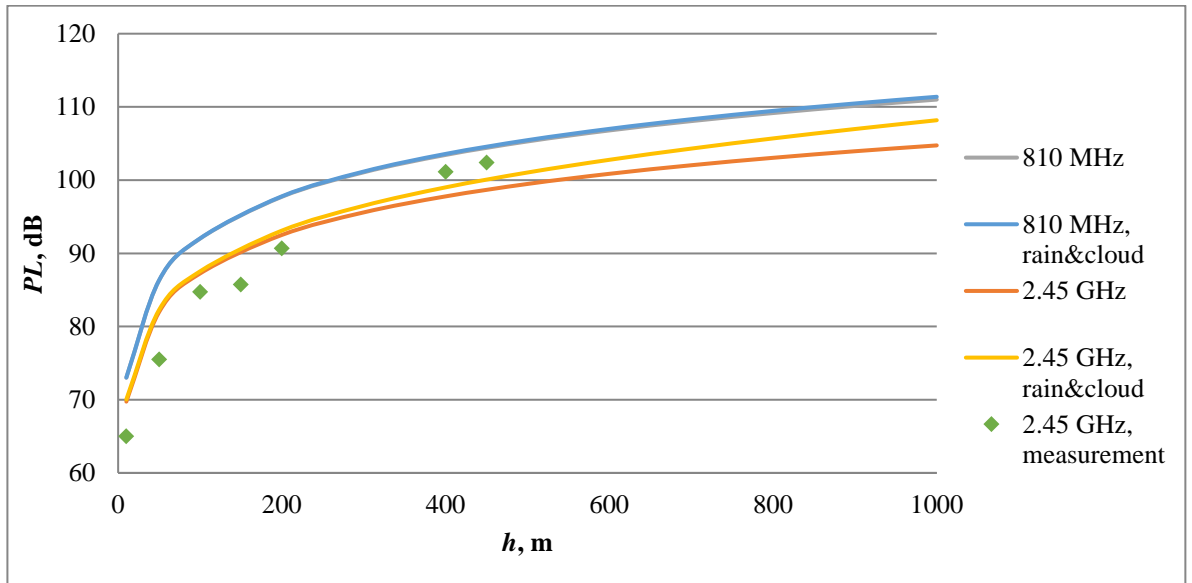


Fig. 18. Experiment data compared with the model

5.8. Analysis of the signal propagation model

Further analysis of ε has shown that its variation depends on both σ , and ζ , and initial transmitter parameters, frequency, and distance. This means ε is a complex function of the earlier mentioned parameters (Fig. 19 and 20).

The correlation coefficient CORR between PL and ε was calculated. When the signal frequency $f = 2.45$ GHz, for all σ and ζ correlation coefficient $CORR \approx 0.998$. Meanwhile, for the frequency $f = 810$ MHz, this correlation coefficient was $CORR_{\min} \approx 0.90$, when $\sigma = 2$ and $\zeta = 0.5$ and $CORR_{\max} \approx 0.995$, when $\sigma = 6.2$ and $\zeta = 6.2$. As we can see, the correlation coefficient is very high, which indicates a

strong relationship between PL and ε . Similarly, there is a correlation between σ and ε : the lowest correlation coefficient, regardless of frequency, is at $\zeta = \sigma$ and is $CORR_{\min} \approx 0.931$, and the maximum coefficient is $CORR_{\max} \approx 0.963$, when $\zeta = 1$.

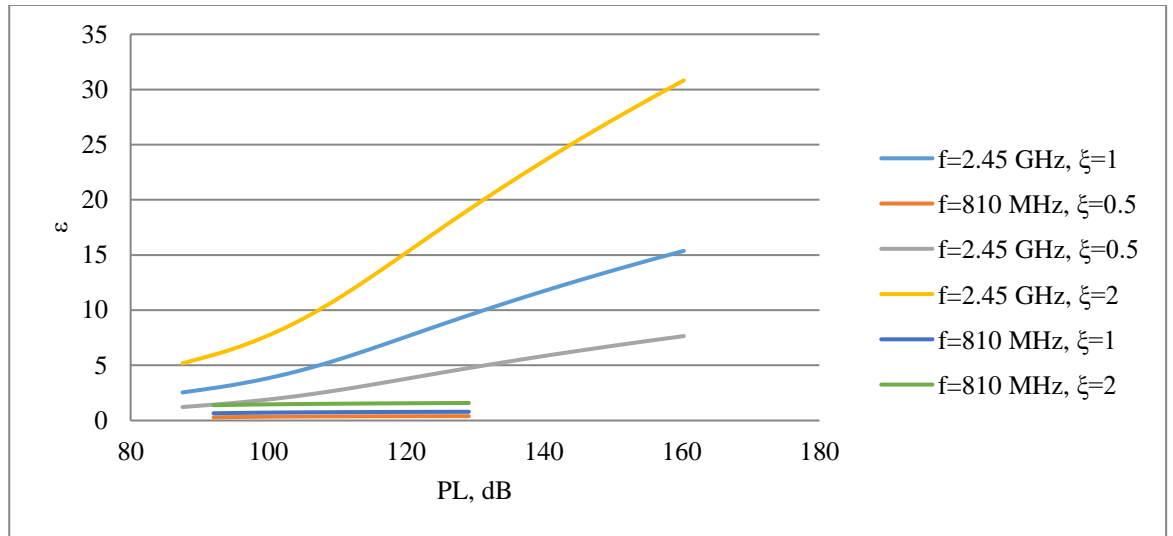


Fig. 19. ε relation to path losses, when $\sigma = 2$ dB

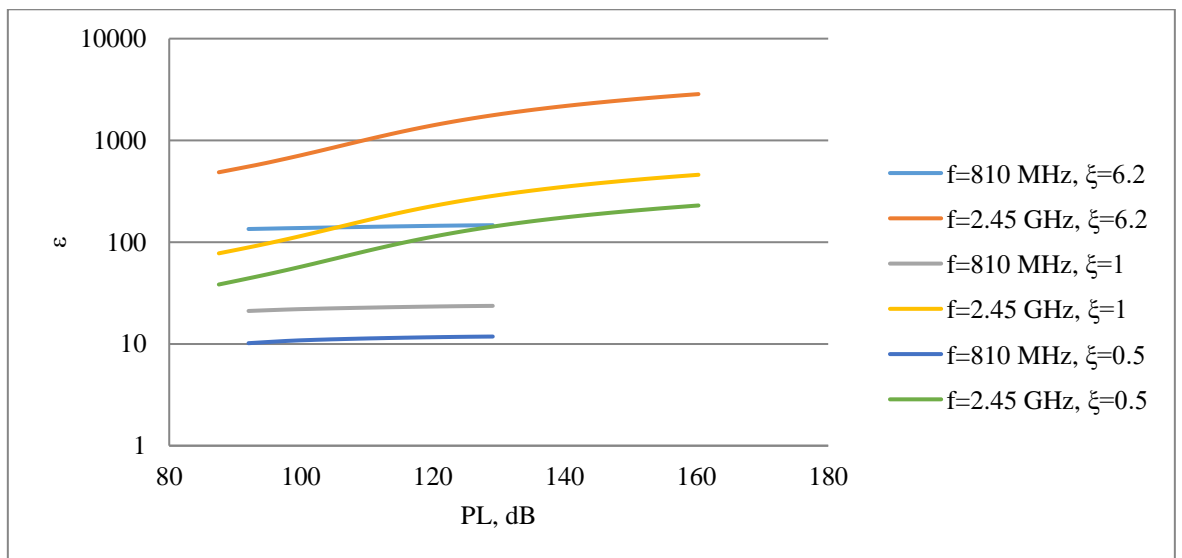


Fig. 20. ε relation to path losses, when $\sigma = 6.2$ dB

At low frequencies, ε is also low and its variation is close to linear variation especially for larger σ . The attempt to approximate these curves was unsuccessful because, as mentioned, it is a rather complex function requiring a separate study. It can only be stated that increasing σ , ζ , PL , parameter ε has a clear increasing trend.

The final model was analysed using statistical analysis methods. Figure 21 shows the dependency of CDF function change on frequency and σ . Because of normal distribution was used for analysis, the CDF was not dependent on ζ . As expected, the results show that the smaller σ cumulative function CDF is steeper, the results are less scattered and the difference $\Delta CDF = CDF_{0.1} - CDF_{0.9}$ corresponds to the narrower ΔPL .

We can also see that the increase in frequency from 810 MHz to 2.45 GHz has no significant impact on the scattering of results.

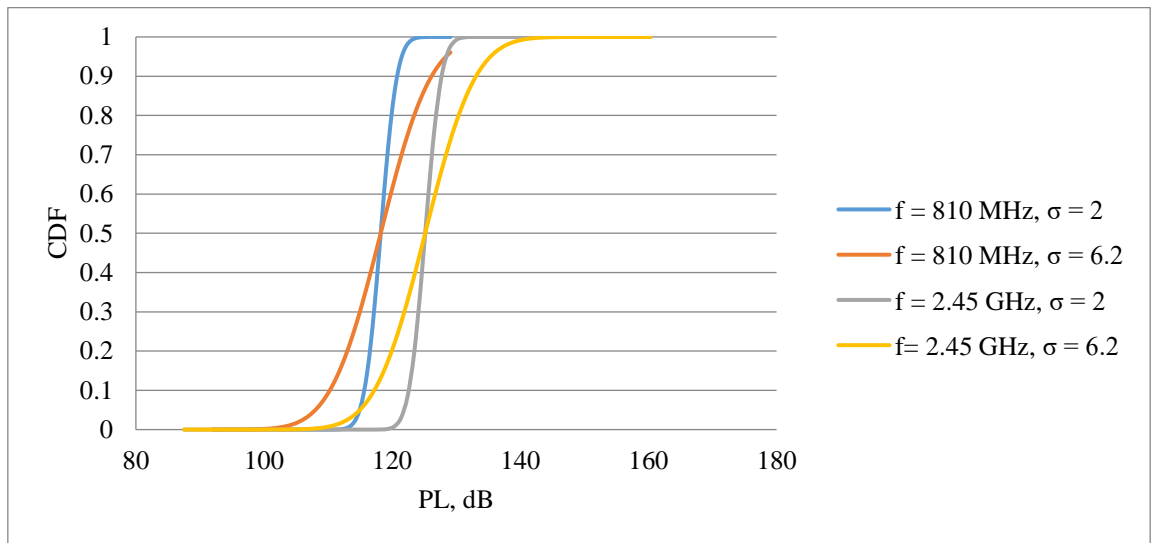


Fig. 21. Cumulative distribution function

The PDF function also matches these results. As we can see from Figure 22, with small σ values, the PDF feature has a sufficiently high peak, and at the same time means that it has less scattering of the results.

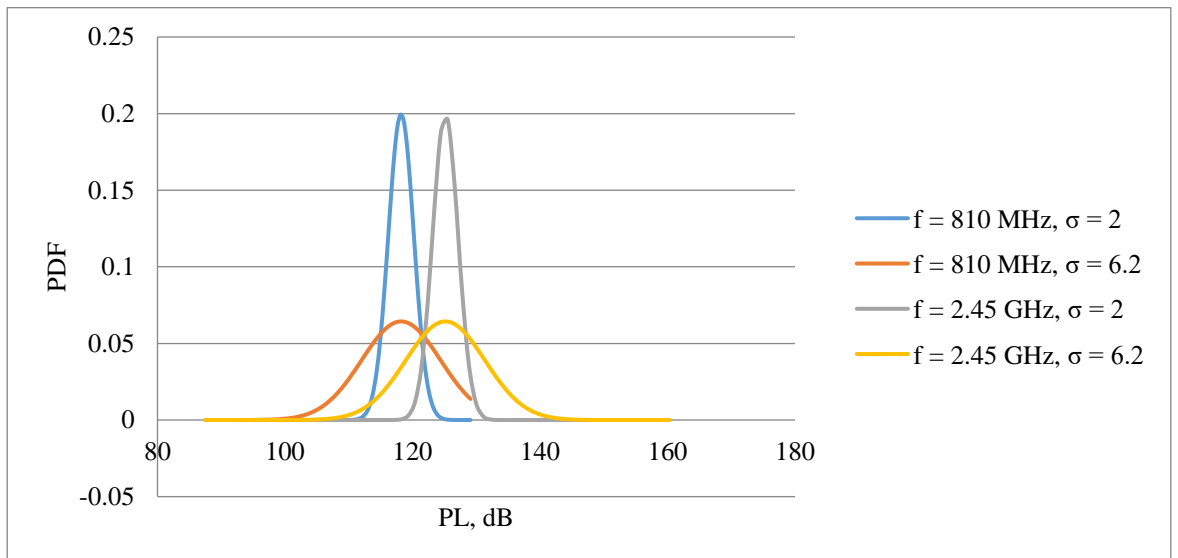


Fig. 22. Probability density function

Conclusions

1. The GOS elements comparison revealed that the air-deployed UAV system is the best option to observe low layers of the atmosphere, especially when investigating storm clouds profile.
2. It has been found that the shape of the object and its attitude impacts the drag coefficient mostly. Also, it must be ensured that the viscosity and compressibility effects, and the Reynolds number or Mach are the same for all the models.
3. The literature analysis shows that the rain and cloud impact are assessed using the formulas proposed by ITU-R Recommendation. It suggested to use the concept of effective distance d_{eff} factor for rain impact analysis. The influence of clouds is considered as an entirety of water droplets, on the propagation of high-frequency waves (> 800 MHz).
4. It is noticed that the base shape of octahedron for the dropsonde is the most balanced figure, and the streamer tail helps to slow down and distribute the flow field during fall equally. It helped to reduce the flow velocity, before the streamer tail was added the results was from 3.310 to 0.995 m/s, and after from 3.00 m/s to 0.691 m/s.
5. The Path losses predicting signal propagating model was created in frequencies $f = 810$ MHz and $f = 2.45$ GHz including rain and cloud impact. The proposed model is based on normal distribution stochastic differential equation. This model can accurately describe the loss of the propagation path by selecting a free member ε . The predicted propagation losses are very sensitive to the change of the free member ε . The analysis of CDF and PDF functions demonstrate that the model meets the statistical characteristics of such signal propagation, in both cases the peak is reached at about 120 dB of path losses.

Discussion

Literature analysis shows that the unmanned aircraft can operate in the lower atmospheric boundary layer of the troposphere, the first several hundred feet above the ground, which is where most weather events that concern humans occur. This atmospheric layer is too low to be studied reliably and safely with manned aircraft. The goal to gather meteorological data and investigate signal propagation will be achieved by combining UAV and dropsonde systems.

It has been found that when propagating UAV signals in hazardous atmospheric conditions it is unreasonable to use a log-normal path propagation model to propagate this signal, as the propagation of the signal due to rain and clouds deviates from the pattern of this model.

The predicted propagation losses are very sensitive to the change of the free member ε . The dependence of its variation is a rather complicated function, depending on such factors as the standard square deviation σ , white noise ζ , signal frequency, signal parameters. Although the tendency of ε change is clear, more detailed research is needed to create its mathematical model.

Further research will focus on real experiments in hazardous weather conditions trying to achieve higher altitudes of the atmosphere up to 3 km using VTOL UAV and 3D printed dropsonde.

List of references

1. Boer, G.; Palo1, S.; Argrow, B.; LoDolce1, G.; Mack, J.; Gao, R.; Telg1, H.; Trussell1, C.; Fromm, J.; Long1, C.N.; Bland, G.; Maslanik, J.; Schmid, B.; Hock, T. *The Pilatus unmanned aircraft system for lower atmospheric research*. 2016. *Atmos. Meas. Tech.*, 9, 1845–1857 p.
2. Schuyler, T.J.; Guzman, M.I. *Unmanned Aerial Systems for Monitoring Trace Tropospheric Gases*. 2017. *Atmosphere*, 8, 206 p.
3. Chilinski, M.T.; Markowicz, K.M.; Kubicki, M. *UAS as a Support for Atmospheric Aerosols Research: Case Study*. 2018. *Pure Appl. Geophys.* 175, 3325–3342 p.
4. World Meteorological Organisation. *Global Planning* [online]. 2020 [viewed 12 January 2020]. Available from: <https://public.wmo.int/>
5. Kelly, G.; Thepaut, J. N. *Evaluation of the impact of the space component of the Global Observing System through Observing System Experiments*. 2007. European Centre for Medium-Range Weather Forecasts Shinfield Park, Reading, UK.
6. Andersson, E. *How to evolve global observing systems*. 2017. ECMWF Newsletter No. 153
7. ITU-R. *Technical Characteristics and Performance Criteria For Radiosonde Systems In The Meteorological Aids Service*. 1997. Radiocommunication Study Group.
8. Wildcard weather. *Radiosondes (weather balloons) and their role in forecasting*. [online]. 2012 [viewed 12 January 2020]. Available from: <https://wildcardweather.com/>
9. Boover, M. *Drones are being used for weather forecasting*. 2016.
10. Vaisala. 2018. *Accuracy Matters in Radiosonde Measurements*.
11. Liu, J.; Tian, J., Yan, D. *Evaluation of Doppler radar and GTS data assimilation for NWP rainfall prediction of an extreme summer storm in northern China: from the hydrological perspective*. 2018. Center for Scientific Computation in Imaging.
12. Lawrence, R. F.; Galinsky, V. L. *Dynamic Multiscale Modes of Severe Storm Structure Detected in Mobile Doppler Radar Data by Entropy Field Decomposition*. 2017. *Journal of Atmospheric Science*.
13. Doviak, R. J.; Zrnicek, D. S.; *Radar Meteorology: Beam propagation*. 1993. *ATMS* 410.
14. Gallo, K. P. *Satellite-Based Adjustments for the Urban Heat Island Temperature Bias*. 1999. *Journal Of Applied Meteorology*.
15. Korean Meteorological Administration. *Sattelite Observation* [online]. 2009. [viewed 16 January 2020]. Available from: <https://www.kma.go.kr/>
16. Tetzlaff, A.; Lupkes C.; Hartmann, J. *Aircraft-based observations of atmospheric boundary-layer modification over Arctic leads*. 2015. *Quarterly Journal of the Royal Meteorological Society*.
17. Nesterov, A. *Aircraft-based Observations* [online]. 2020 World Meteorological Organisation. [viewed 12 January 2020]. Available from: <https://public.wmo.int/>
18. WMO. *The AMDAR Observing System*. 2017. AMDAR resources standards.
19. M. Buschmann, J. Bange, P. Mmav. *A Miniature Unmanned Aerial Vehicle (Mini-Uav) For Meteorological Purposes*. Vörsmann Technische Universität Braunschweig, Germany
20. Z. Bottyán, F. Wantuch, A. Z. Gyöngyösi, Z. Tuba, K. Hadobács, P. Kardos, and R. Kurunczi. *Development of a Complex Meteorological Support System for UAVs*. 2013. World Academy of Science, Engineering and Technology International Journal of Geological and Environmental Engineering.
21. Shashank, S.; Vaibhav, N. *Weather Monitoring Unmanned Aerial Vehicle*. 2014. *Advanced Research in Electrical and Electronic Engineering*.

22. Schmid, L. *Dropping in on a Hurricane*. 2007. Global Hydrology Resource Center.
23. Omar, A.; Meer B.; Bergman, E.; Lamber, J. *Analysis of Currents via Aerial Navigation*. 2018. ASEN 4018
24. MESO. *Next-Generation Wireless Sensor System for Environmental Monitoring*. 2013. Inc., Grant IIP
25. Glenn research center. *Free-falling objects*. National Aeronautics and Space Administration. 2010.
26. Ellermeyer, S. F. *Falling Objects*. 2003.
27. Conrad, B. P. *Ordinary Differential Equations: A Systems Approach*. 2010
28. Ramachandran, R. *Surface Structure and Its Effect on Reducing Drag*. 2015. College of Engineering Department of Aerospace Engineering.
29. Hoerner, S.F., *Fluid-Dynamic Drag*. 2nd ed., Hoerner Fluid Dynamics, Bricktown, NJ, June 1965.
30. Khawaja, W.; Guvenc, I.; Matolak, D.W.; Fiebig, U.C.; Schneckenberger, N. *A Survey of Air-to-Ground Propagation Channel Modeling for Unmanned Aerial Vehicles*. 2018. arXiv:1801.01656v1 [eess.SP].
31. Amorim, R.; Mogensen, H.N.P.; Kovács, I.Z.; Wigard, J.; Sørensen, T.B. *Radio Channel Modeling for UAV Communication Over Cellular Networks*. 2017. IEEE Wireless Communications Letters, VOL. 6, NO. 4, 514 p.
32. Amorim, R.M.; Mogensen, P.E.; Sørensen, T.B.; Kovács, I.; Wigard, J. *Pathloss Measurements and Modeling for UAVs Connected to Cellular Networks*. 2017. IEEE 85th Vehicular Technology Conference (VTC Spring).
33. Venkatasubramanian, S.N. *Propagation channel model between unmanned aerial vehicles for emergency communications*. 2013. AALTO University School Of Electrical Engineering.
34. Peng, J. *The Shadowing Propagation Model In Unmanned Aerial Vehicle Networks*. 2015. Electrical Engineering Department University of Texas.
35. Yanmaz, E.; Kuschnig, R.; Bettstetter, C. *Channel Measurements over 802.11a-based UAV-to-Ground Links*. 2011. IEEE Globecom-WiUAV.
36. Zhi Yang, Z.; Zhou, L.; Zhao, G.; Zhou, S. *Channel Model in the Urban Environment for Unmanned Aerial Vehicle Communications*. 2018. arXiv:1805.04328v1 [cs.IT].
37. Al-Hourani, A. *Modeling Cellular-to-UAV Path-Loss for Suburban Environments*. 2017. IEEE Wireless Communication Letters.
38. Kulikov, G.; Nesterov, A.; Leluh, A. *Simulation of the Radio Communication Channel with Unmanned Aerial Vehicle in Urban Conditions*. 2018. Journal of Electrical and Electronic Engineering 105 p.
39. Nagendra Sah, N.; Thakur, T. *Effect of Clutters on Path Loss Proposed by Walfisch-Ikegami Propagation Model*. Available from: <http://www.ncc.org.in/download.php?f=NCC2005/S18-03.pdf>
40. Ho, C.M.; Wang, C.; Angkasa, K.; Gritton, K. *Estimation of Microwave Power Margin Losses Due to Earth's Atmosphere and Weather in the Frequency Range of 3–30 GHz*. 2004. Edwards Air Force Base, California.
41. Kakar, J.A. *UAV Communications: Spectral Requirements, MAV and SUAV Channel Modelling, OFDM Waveform Parameters, Performance, and Spectrum Management*. 2015. Faculty of the Virginia Polytechnic Institute and State University.
42. Solidworks. Available from: <https://www.solidworks.com/>

43. Chueh, C.; Wang, P. K.; Hashino, T. *Numerical Study of Motion of Falling Conical Graupel*. 2017. Atmospheric Research 199.
44. Мееров И.Б., Сысоев А.В. *Лабораторная работа Численное решение стохастических дифференциальных уравнений на примере модели рования финансово горынка*. 2011. Нижегородский государственный университет.
45. Вохник, О.М.; Зотов, А.М.; Короленко, П.В.; Рыжикова, Ю.В. *Моделирование и обработка стохастических сигналов и структур*. 2013. Московский Государственный Университет.
46. Cai, X.; Pineiro, J. R.; Yin, X. *An Empirical Air-to-Ground Channel Model Based on Passive Measurements in LTE*. 2019. IEEE.
47. Cheng, K. Y.; Wang, P. K.; *A Numerical Study on the Attitudes and Aerodynamics of Freely Falling Hexagonal Ice Plates*. 2015. American Meteorological Society.

Appendices

Appendix 1. Coefficients of drag of the shapes

Cylinder.SLDPRT

Goal Name	Unit	Value	Average Value	Minimum Value	Maximum Value	Progress [%]	Use In Convergence	Delta	Criteria
GG Force (Y) 1	[N]	0.014268057	0.014253045	0.014194224	0.014273106	100	Yes	7.8882E-05	0.000116783
Equation Goal 1	[]	0.16459091	0.164417736	0.163739199	0.164649152	100	Yes	0.000909953	0.001347168

Iterations

[]: 135

Analysis

interval: 37

Cone.SLDPRT

Goal Name	Unit	Value	Average Value	Minimum Value	Maximum Value	Progress [%]	Use In Convergence	Delta	Criteria
GG Force (Y) 1	[N]	0.010823748	0.011370257	0.010771061	0.012055052	100	Yes	0.000359624	0.000426946
Equation Goal 1	[]	0.124858669	0.131162983	0.124250894	0.139062522	100	Yes	0.004148482	0.004925086

Iterations

[]: 80

Analysis

interval: 35

Cube.SLDPRT

Goal Name	Unit	Value	Average Value	Minimum Value	Maximum Value	Progress [%]	Use In Convergence	Delta	Criteria
GG Force (Y) 1	[N]	0.015259603	0.015097306	0.014478286	0.015278333	100	Yes	0.000365754	0.00039223
Equation Goal 1	[]	0.176029014	0.174156813	0.167016038	0.176245072	100	Yes	0.0042192	0.004524616

Iterations

[]: 131

Analysis

interval: 38

Cuboid.SLDPRT

Goal Name	Unit	Value	Average Value	Minimum Value	Maximum Value	Progress [%]	Use In Convergence	Delta	Criteria
GG Force (Y) 1	[N]	0.007339264	0.007315997	0.007262375	0.007339553	100	Yes	7.71782E-05	7.72583E-05
Coefficient of Drag	[]	0.084662974	0.084394573	0.083776014	0.084666313	100	Yes	0.000890299	0.000891223

Iterations []: 145
 Analysis interval: 39

Dodecahedron.SLDPRT

Goal Name	Unit	Value	Average Value	Minimum Value	Maximum Value	Progress [%]	Use In Convergence	Delta	Criteria
GG Force (Y) 1	[N]	0.011173901	0.011215993	0.01110582	0.011392796	100	Yes	0.000286976	0.000325941
Equation Goal 1	[]	0.128897893	0.129383454	0.128112541	0.131422983	100	Yes	0.003310442	0.003759931

Iterations []: 75
 Analysis interval: 36

Ellipsoid.SLDPRT

Goal Name	Unit	Value	Average Value	Minimum Value	Maximum Value	Progress [%]	Use In Convergence	Delta	Criteria
GG Force (Y) 1	[N]	0.004735886	0.004719563	0.004665695	0.004772317	100	Yes	0.000106622	0.000117113
Equation Goal 1	[]	0.054631394	0.054443094	0.053821693	0.055051645	100	Yes	0.001229951	0.001350966

Iterations []: 91
 Analysis interval: 39

Hexahonal pyramid.SLDPRT

Goal Name	Unit	Value	Average Value	Minimum Value	Maximum Value	Progress [%]	Use In Convergence	Delta	Criteria
GG Force (Y) 1	[N]	0.030779217	0.031070025	0.030112272	0.031468783	100	Yes	0.001356511	0.001521113
Equation Goal 1	[]	0.355057417	0.358412063	0.347363791	0.36301199	100	Yes	0.015648199	0.017546989

Iterations

[]: 139

Analysis

interval: 32

Hexagonal prism.SLDPRT

Goal Name	Unit	Value	Average Value	Minimum Value	Maximum Value	Progress [%]	Use In Convergence	Delta	Criteria
GG Force (Y) 1	[N]	0.021200226	0.021141509	0.02101155	0.021200226	100	Yes	0.000188676	0.00019366
Equation Goal 1	[]	0.24455779	0.243880462	0.242381298	0.24455779	100	Yes	0.002176492	0.002233992

Iterations

[]: 158

Analysis

interval: 36

Icosahedron.SLDPRT

Goal Name	Unit	Value	Average Value	Minimum Value	Maximum Value	Progress [%]	Use In Convergence	Delta	Criteria
GG Force (Y) 1	[N]	0.011868712	0.011812141	0.011722078	0.011868712	100	Yes	4.38612E-05	5.19554E-05
Equation Goal 1	[]	0.136912971	0.136260388	0.135221461	0.136912971	100	Yes	0.000505967	0.000599338

Iterations

[]: 99

Analysis

interval: 37

Octahedron.SLDPRT

Goal Name	Unit	Value	Average Value	Minimum Value	Maximum Value	Progress [%]	Use In Convergence	Delta	Criteria
GG Force (Y) 1	[N]	0.012068537	0.011560136	0.011103808	0.012197113	100	Yes	0.000237612	0.000261916
Equation Goal 1	[]	0.139218077	0.133353361	0.128089337	0.140701287	100	Yes	0.002741002	0.00302136

Iterations

[]: 105

Analysis

interval: 38

Pentagonal prism.SLDPRT

Goal Name	Unit	Value	Average Value	Minimum Value	Maximum Value	Progress [%]	Use In Convergence	Delta	Criteria
GG Force (Y) 1	[N]	0.017723355	0.018197837	0.016961148	0.019819589	100	Yes	0.000293005	0.000305181
Equation Goal 1	[]	0.20444992	0.209923364	0.195657389	0.228631282	100	Yes	0.003379994	0.003520451

Iterations

[]: 99

Analysis

interval: 36

Sphere.SLDPRT

Goal Name	Unit	Value	Average Value	Minimum Value	Maximum Value	Progress [%]	Use In Convergence	Delta	Criteria
GG Force (Y) 1	[N]	0.005723674	0.005715512	0.00569215	0.005726393	100	Yes	3.42435E-05	0.000312445
Equation Goal 1	[]	0.066026139	0.065931986	0.065662488	0.066057509	100	Yes	0.00039502	0.003604251

Iterations

[]: 72

Analysis

interval: 36

Square pyramid.SLDPRT

Goal Name	Unit	Value	Average Value	Minimum Value	Maximum Value	Progress [%]	Use In Convergence	Delta	Criteria
GG Force (Y) 1	[N]	0.013182838	0.012133735	0.010308033	0.013182838	100	Yes	0.00148182	0.001714524
Equation Goal 1	[]	0.152072238	0.139970181	0.118909575	0.152072238	100	Yes	0.017093714	0.019778095

Iterations []: 84
Analysis interval: 37

Tetrahedron.SLDPRT

Goal Name	Unit	Value	Average Value	Minimum Value	Maximum Value	Progress [%]	Use In Convergence	Delta	Criteria
GG Force (Y) 1	[N]	0.007936011	0.007880898	0.007662102	0.007936012	100	Yes	0.000274019	0.000283703
Equation Goal 1	[]	0.091546824	0.09091106	0.088387109	0.091548083	100	Yes	0.003160974	0.003272694

Iterations []: 115
Analysis interval: 33

Triangular prism.SLDPRT

Goal Name	Unit	Value	Average Value	Minimum Value	Maximum Value	Progress [%]	Use In Convergence	Delta	Criteria
GG Force (Y) 1	[N]	0.003898857	0.00382369	0.003769063	0.003904485	100	Yes	0.000135422	0.000287138
Equation Goal 1	[]	0.044975736	0.044108642	0.043478488	0.045040664	100	Yes	0.001562176	0.00331231

Iterations []: 91
Analysis interval: 46